Schweizerische Eidgenossenschaft
Confédération suisse
Confederazione Svizzera
Confederaziun svizra

Federal Department of the Environment, Transport,
Energy and Communications DETEC

Swiss Federal Office of Energy SFOE
Energy Research and Cleantech Division

REEL Demo – Romande Energie ELectric network in local balance Demonstrator

Deliverable: 2a2 Identification and Validation of dynamic grid model for distributed controller strategy

Demo site: Aigle

Developed by
Alireza Karimi, Sohail Madani, Christoph Kammer
Laboratoire d'Automatique, EPFL
In Collaboration with
Monash University, Melbourne

[Lausanne, 28.03.2021]

1. Description of deliverable and goal

1.1. Executive summary

The displacement of synchronous power plants by renewable energy resources (RESs) is causing a significant reduction of inertia in power systems. This will change significantly the dynamics of the electrical grid and can lead to large oscillations in voltage and frequency. The objective of this project is to analyze the impact of the integration of distributed generation (DG) units into power grids and propose the feedback control solutions to guarantee the frequency and voltage stability as well as active and reactive power sharing among the distributed generation units. A data-driven methodology is used to identify a large set of models for different system configurations using the Phasor Measurement Units (PMUs) data. The models are then classified according to some scheduling parameters which are estimated in real-time operation from PMUs data. New centralised and distributed control algorithms are developed that are robust with respect to the variation of the scheduling parameters or adapted in real-time using the estimated dynamics.

1.2. Research question

Modeling and control of electrical grids has become a more challenging issue due to the increasing penetration of renewable energy sources, changing system structure and the integration of new storage systems, controllable loads and power electronics technologies, and reduction of system inertia. Conventional modelling and control designs may not be anymore effective to satisfy all specified objectives in various operation modes of modern power grids. These challenging issues set new demand for development of more flexible, rapid, effective, precise, and adaptive approaches for power system dynamic monitoring, stability/security analysis, and control problems. The power system is a nonlinear multivariable time-varying system. It is represented by a nonlinear set of equations for the generators (swing equations), for the transmission lines and for the loads, which for a typical power system has a few hundreds of states. For the control design purpose, usually a reduced-order linearized model around an operating point is used and it is assumed that all system parameters are known and time-invariant. These assumptions, however, are not valid in a real power system with dominated DGs/RESs. The main dynamic modes of the system are varying stochastically during a day because of the variation of load and aggregated inertia. The dynamic modes will change more significantly by integration of the new RESs into the power system. Therefore, a fixed linearized time-invariant model will not represent correctly the behaviour of the power system.

1.3. Novelty of the proposed solutions compared to the state-of-art

Model identification in power systems is a widely investigated topic. Primarily, two main approaches exist in data-driven power system model identification. First approach is model identification through disturbances where a model is identified based on the step disturbances such as generator trippings, load trippings and line disconnections or using ambient data in normal operating conditions that are treated as stochastic white noise disturbances. One drawback of treating ambient data as stochastic white noise disturbances is that the data have to be recorded for a long time interval to have a persistently excitation signal. Therefore, in this project the system is excited by a probing signal. Usually, a signal-injection-based method is used for experimentally identifying the reduced order model of the power system using parametric system identification methods. These models are typically used to tune the controllers. In contrast, in this project, a computationally efficient discrete-Fourier-transform-based method is used to identify the frequency response of the system using the measured data of PMUs. This method eliminates the need for prior knowledge of the power system and its components such as equipment and their configurations, topology, and operating conditions. Then a novel framework that designs fixed-structure robust controllers for grid-supporting BESSs based on the experimentally identified frequency response is proposed and the efficacy of the proposed framework is validated in a real-time hardware-in-the-loop testbed that is equipped with a PMU. Thereby, practical aspects such as variable delays and uncertainties in the communication network are inherently taken into account.

1.4. Description

The detailed description of the deliverables are presented in Appendix A to Appendix D. A summary of the results are given here :

Appendix A: A comprehensive data-driven distributed combined primary/secondary controller design method for microgrids is proposed. This method provides transient and steady-state performances, including power sharing and voltage and frequency restoration while guaranteeing stability for fixed communication delays. Measured data are directly used for controller design, and no knowledge of the model structure or the physical parameters of the grid is required. Moreover, no assumption is made on the X/R ratio of the feeders. All control specifications are formulated as frequency-domain constraints on the two-norm of weighted sensitivity functions. Then, using a frequency-domain robust control design method, a distributed fixed-structure controller is synthesized in one step. The performance of the obtained controller is validated using hardware-in-the-loop (HIL) experiments. The results show considerable improvement in transient performance while providing power sharing and voltage and frequency restoration with a distributed implementation.

Appendix B: A data-driven multivariable Linear Parameter Varying (LPV) controller design method is proposed. The synthesis process is based on frequency-domain data corresponding to different operating points of the power grid. The H∞ performance and also stability constraints for frozen scheduling parameter are convexified around an initial stabilizing controller and solved using a convex optimization solver. This method has been applied to the combined primary and secondary controller design problem of electrical microgrids. The performance of the proposed method has been validated through simulating a microgrid including a synchronous generator, a battery storage and a photo-voltaic unit. The results show that using this method, high performance is achieved in different operating points.

Appendix C: Reactive power sharing for Photo- voltaic (PV) units in islanded microgrids is formulated as a robust control design problem and is solved using convex optimization method. In addition to reactive power sharing, the disturbance rejection for voltage and active power are formulated using infinity-norm constraints on the sensitivity functions and considered in the design. The proposed method uses only the measurement data of the power system with no need for a parametric model of the power grid equipment. The size of the problem is independent of the order of the plant which makes it applicable to power systems including a high number of buses and equipment such as synchronous generators, batteries and inverters. In the proposed method, the communication system can be considered in the control design process for centralized, distributed and decentralized structures. The proposed method has been validated through simulation of a microgrid encompassing synchronous generator, switching inverters and storage system. The results show that this method has successfully shared reactive power among different PV units while providing disturbance rejection for voltage and active power.

Appendix D: Fast responding services, such as battery energy storage systems (BESSs), are increasingly getting deployed to deal with large frequency excursions that take place in low-inertia power systems. This project proposes a novel wide area monitoring system based robust controller framework for BESSs to control the frequency in low-inertia grids. To overcome the modeling errors, this framework depends on an experimentally identified nonparametric model from synchrophasors. Further, an optimization-based robust fixed-structure control design method is adopted to tune the controller gains. The objective function, the infinity norm of the output sensitivity function, is minimized to enhance disturbance rejection while being subjected to performance constraints such as control effort and steady-state gain to achieve the required performance. The performance and efficacy of the proposed controller framework are validated through real-time hardware-in-the-loop experiments based on an Opal RT platform simulating the southeastern power system of Australia. The performance of the designed controller based on the framework is compared with that of a conventional droop controller for a variety of different cases.

1.5. Regulatory and legal barriers for implementation

There is no legal barrier for grid model identification using measured data. However, smart measuring units are required for data acquisition in the controlled busses. A sampling rate of at least one millisecond and high precision measurements (even in short periods) are required for dynamic model identification.

2. Achievement of deliverable:

2.1. Date

The deliverable is achieved in 2020.

2.2. Demonstration of the deliverable

The proposed method has been validated by Hardware-In-the-Loop (HIL) simulation for an IEEE standard power grid, a shipboard islanded microgrid and the southeastern power system of Australia.

3. Impact

This deliverable is related to Subtask 1.2: Real-time control strategies for heterogeneous resources at MV and LV. This work has been done in collaboration with Power Engineering Advanced Research Laboratory (PEARL) in Monash University, Melbourne, Australia. The results have been accepted to be published in IEEE Transactions on Control Systems Technology and presented in international conferences (see Appendices).

APPENDIX A

Data-Driven Distributed Combined Primary and Secondary Control in Microgrids

Published in IEEE Transactions On Control Systems Technology (2021)

Data-Driven Distributed Combined Primary and Secondary Control in Microgrids

Seyed Sohail Madani, Christoph Kammer, Alireza Karimi

***Abstract*—This paper presents a comprehensive data-driven distributed combined primary/secondary controller design method for microgrids. This method provides transient and steady-state performance including power-sharing and voltage and frequency restoration while guaranteeing stability for fixed communication delay. The measured data is directly used for controller design with no need for knowledge about the order or structure of the system and grid physical parameters. Moreover, no assumption is made on X/R-ratio of feeders. All the control specifications are formulated as frequency-domain constraints on the 2-norm of weighted sensitivity functions. Then, using a recently developed frequency-domain robust control design method, a distributed fixed-structure controller is synthesized in one step. The performance of the obtained controller is validated using Hardware-In-the-Loop (HIL) experiments. The results show considerable improvement in transient performance, while providing power-sharing and voltage and frequency restoration using distributed implementation.**

***Index Terms*—Data-driven controller design, frequency control, voltage control, power-sharing, microgrid control, distributed control.**

I. Introduction

GLOBAL warming and imposing limitation on greenhouse gas emission have led to the increase of renewable generation penetration in electrical grids. In order to facilitate the integration of renewable Distributed Generation units (DGs) and Energy Storage Systems (ESSs), the idea of microgrid has been proposed. A microgrid is a small distribution power system that includes its own DGs, ESSs and loads. It has the capability to operate autonomously (islanded mode) or in grid-connected mode. As a consequence of the penetration of renewable energy resources, microgrids suffer from low inertia and high fluctuation of generation. The microgrid control is known as a challenging problem and has been widely studied in the literature [1]. The main expected features of an efficient microgrid control system include providing power-sharing, voltage and frequency steady-state disturbance rejection, voltage and frequency transient performance while guaranteeing stability.

Droop control [2] is the most well-known method for power-sharing in microgrids with dominant inductive or resistive feeders. This method shares power proportionally among DGs based on the frequency deviation and has been popular because of being model-free, very simple and decentralized. However, the major drawbacks are the steady-state errors in voltage and frequency as well as poor transient performance. Moreover, even power-sharing is not achieved for most of distribution grids where the feeders are not dominantly resistive or inductive [1], [3]. Hierarchical control structure [3], [4] is proposed mainly to improve the steady-state voltage and frequency response by adding a secondary control layer, which should be implemented in a centralized [5] or distributed way [6]. However, conventional secondary layer deteriorates the power-sharing and requires time scale separation between different layers. The low bandwidth of higher layers leads to slow voltage and frequency restoration which may trigger the corresponding protection relays. A solution to this problem is proposed in [7] using a distributed averaging control system. The small-signal stability of these systems is studied in [8], [9]. The nonlinear stability is assessed rigorously for lossy systems in [10] and for lossless systems in [7], [11], [12].

Apart from power-sharing and steady-state voltage and frequency performance, designing controllers to improve the transient performance in microgrids is a major challenge. Having mixed resistive/inductive lines, lack of inertia, and poor transient modeling are main factors affecting the transient performance of the microgrids. Different solutions have been proposed in the literature in this regard. In order to improve the transient performance, one idea is to mimic Synchronous Generator (SG) behavior and provide virtual inertia to the system [13]–[15]. While providing inertia, these methods do not use the capability of inverters as high bandwidth actuators. Another idea is to add an H_∞ robust controller to the primary droop controller [16]. However, when combined with droop controllers, both approaches are based on the questionable assumption on the dominantly resistive or inductive feeders. The use of quadratic droop control, proposed in [17], can improve the performance of the control system for the distribution grids with uniform X/R-ratio of the feeders. Some advanced model-based control techniques combine the primary and secondary control without considering the power-sharing performance [18]–[21].

In the literature, there is a lack of a comprehensive systematic microgrid control synthesis method to provide power-sharing in addition to voltage and frequency restoration and at the same time, improving transient performance for arbitrary X/R-ratio. For filling the mentioned gap, this paper proposes a non-droop based primary/secondary control design method formulated as a convex optimization problem in a data-driven

The authors are with the Laboratoire d' Automatique, École Polytechnique Fédérale de Lausanne (EPFL), 1015 Lausanne, Switzerland. *(Corresponding author: Alireza Karimi (alireza.karimi@epfl.ch).)*

This project is carried out within the frame of the Swiss Centre for Competence in Energy Research on the Future Swiss Electrical Infrastructure (SCCER-FURIES) with the financial support of the Swiss Innovation Agency (Innosuisse - SCCER program). The work of S. S. Madani (e-mail: sohail.madani@epfl.ch) is supported by the Swiss National Science Foundation under Grant 200021_172828.

framework. Only measurement data of the power grid is used in controller synthesis and there is no need for parametric system identification, and no knowledge about the physical parameters of the power system is required. The closed-loop stability is guaranteed for the fixed communication delay using specific fixed terms in the controller structure of distributed controllers.

The performance of the proposed method has been validated through HIL experiment on an islanded microgrid including SG, batteries and PV units interfaced with switching inverters. The distributed controllers are implemented on embedded real-time systems and the microgrid is simulated in a real-time simulator.

The rest of the paper is organized as follows: In Section II, the controller design method is reviewed. Section III shows how the performance specifications for the control of a microgrid can be transformed to frequency-domain convex constraints and integrated into the proposed method. The case study and HIL setup results are given in Section IV followed by some concluding remarks.

II. Control Design by Convex Optimization

A recently developed control design method which is based on the frequency response of multivariable systems and convex optimization is used in this paper. The method can be employed to design fixed-structure controllers for infinite-dimensional systems, which allows the use of frequency response data for controller design. A full theoretical exposition of the method can be found in [22], which is summarized in the sequel.

1) Frequency Response Data: The system to be controlled is a Linear Time-Invariant multivariable (LTI-MIMO) system represented by its frequency response $G(j\omega) \in \mathbb{C}^{n\times m}$, with m inputs and n outputs. $G(j\omega)$ is assumed to be bounded in all frequencies except for a finite set of frequencies B_g, which correspond to the poles of G on the imaginary axis. Further, define $\omega \in \Omega$ with:

$$\Omega = \left\{ \omega \,\middle|\, -\frac{\pi}{T_s} \leq \omega \leq \frac{\pi}{T_s} \right\} \setminus B_g \tag{1}$$

where T_s is the sampling time of the control system. In this paper, frequency ω represents the points in the frequency domain on which Fourier transform is calculated, while the frequency shown by f is the derivative of the electrical angle. For the sake of simplicity, in the rest of the paper, arguments of transfer functions are omitted whenever clear from the context.

2) Controller Structure: Since the design is based on frequency-domain data, it is possible to directly design a discrete-time controller using the frequency response of a continuous-time plant. The controller is defined as $K(z) = X(z)Y(z)^{-1}$, where:

$$\begin{aligned} X(z) &= (\underline{X}_\delta z^\delta + \underline{X}_{\delta-1} z^{\delta-1} + \cdots + \underline{X}_1 z + \underline{X}_0) \circ F_X(z) \\ Y(z) &= (I z^\delta + \underline{Y}_{\delta-1} z^{\delta-1} + \cdots + \underline{Y}_1 z + \underline{Y}_0) \circ F_Y(z) \end{aligned} \tag{2}$$

$X(z)$ and $F_X(z)$ are $m \times n$ and $Y(z)$ and $F_Y(z)$ are $n \times n$ polynomial matrices in z and $\circ$ denotes the element-wise matrix multiplication. $\underline{X}_i \in \mathbb{R}^{m\times n}$ for $i \in \{1, 2, \cdots, \delta\}$ and $\underline{Y}_r \in \mathbb{R}^{n\times n}$ for $r \in \{1, 2, \cdots, \delta - 1\}$ contain controller parameters. $F_X(z)$ and $F_Y(z)$ are the fixed terms of controller.

3) Control Performance: It can be defined as the minimization of the weighted norm of any closed-loop sensitivity function. For example, consider the following performance objective on the output sensitivity function $\mathcal{S} = (I + GK)^{-1}$:

$$\min_K \|W_L \mathcal{S} W_R\|_2 \tag{3}$$

where W_L and W_R are the left and right weighting filters and W_R is invertible. This objective function, for a stable closed-loop system, can be approximated by a semi-definite programming using a frequency grid $\Omega_N = \{\omega_1, \ldots, \omega_N\}$, where $\omega_1 \geq 0$ and $\omega_N = \pi/T_s$:

$$\begin{gathered} \min \sum_{k=1}^{N} \mathrm{tr}(\Gamma_k) \\ (W_{Lk} \mathcal{S}_k W_{Rk})^* \, (W_{Lk} \mathcal{S}_k W_{Rk}) \leq \Gamma_k \ , \ \forall \{k | \omega_k \in \Omega_N\} \end{gathered} \tag{4}$$

where a frequency function with subscript k shows the value of the function at ω_k (e.g. $\mathcal{S}_k = \mathcal{S}(e^{j\omega_k})$). The optimization variables are the controller parameters (the parameters of $X(z)$ and $Y(z)$ i.e. $\underline{X}_i$ for $i \in \{1, 2, \cdots, \delta\}$ and $\underline{Y}_r$ for $r \in \{1, 2, \cdots, \delta - 1\}$) and dummy matrix variables ($\Gamma_k > 0 \in \mathbb{C}^{n\times n}$ for $k = 1, \ldots, N$). Finally, $(\cdot)^*$ denotes the conjugate transpose. Replacing $\mathcal{S}$ with $(I + GXY^{-1})^{-1}$, the constraint is reformulated as:

$$W_{Lk} Y_k \left((W_{Rk}^{-1} M_k)^* (W_{Rk}^{-1} M_k) \right)^{-1} (W_{Lk} Y_k)^* \leq \Gamma_k \tag{5}$$

where $M_k = Y_k + G_k X_k$. Taking the Schur complement yields:

$$\begin{bmatrix} \Gamma_k & W_{Lk} Y_k \\ (W_{Lk} Y_k)^* & (W_{Rk}^{-1} M_k)^* (W_{Rk}^{-1} M_k) \end{bmatrix} \geq 0$$

for $k = 1, \ldots, N$. In [22], it is shown that the quadratic part in the lower right can be linearized around $M_{ck} = Y_{ck} + G_k X_{ck}$ where $K_c = X_c Y_c^{-1}$ is a stabilizing initial controller. This leads to a convex optimization problem with Linear Matrix Inequality (LMI) constraint as follows:

$$\begin{gathered} \min \sum_{k=1}^{N} \mathrm{tr}(\Gamma_k) \\ \begin{bmatrix} \Gamma_k & W_{Lk} Y_k \\ (W_{Lk} Y_k)^* & \mathbf{M}_{Wk} \end{bmatrix} \geq 0 \ , \ \forall \{k | \omega_k \in \Omega_k\} \end{gathered} \tag{6}$$

where

$$\begin{aligned} \mathbf{M}_{W_k} &= M_{Wk}{}^* M_{W_{ck}} + M_{W_{ck}}{}^* M_{W_{ck}} - M_{W_{ck}}{}^* M_{W_{ck}} \\ M_{Wk} &= W_{Rk}^{-1} M_k \qquad ; \qquad M_{W_{ck}} = W_{Rk}^{-1} M_{ck} \end{aligned}$$

If the following conditions are satisfied, the final controller K will be a stabilizing controller:

1) $\det(Y) \neq 0, \forall \omega \in \Omega$.
2) The initial controller K_c and the final controller K share the same poles on the stability boundary.
3) The order of $\det(Y)$ is equal to the order of $\det(Y_c)$.

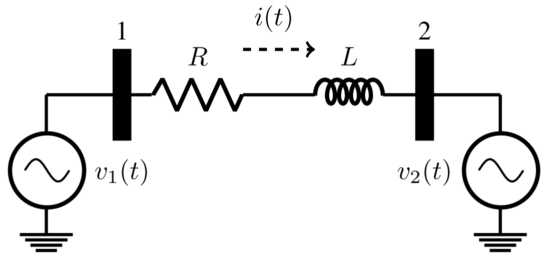

Fig. 1. Single line diagram of a two-node power system

TABLE I
DESCRIPTION OF THE TRANSFER FUNCTIONS USED IN FIG. 2

K_{PID}	SG internal speed controller
$G_{S,m}$	from mechanical reference of SG to its mechanical angular frequency
$G_{S,e}$	from SG output electrical power to its mechanical angular frequency
$G_{I,f}$	from inverter frequency reference to its frequency
$G_{I,V}$	from inverter voltage reference to its output voltage
$G_{S,V}$	equivalent closed-loop response of SG AVR
G_{grid}	from the power grid nodal voltage and frequency to injected active active and reactive power
G_d	from load power to power drawn at DG nodes
K	MIMO controller

III. PRIMARY-SECONDARY CONTROL DESIGN PROBLEM

In this paper, the frequency response of the Dynamic Phasor Model (DPM) of the microgrid is used for the controller design. For the first time, DPM was proposed in [23] and is used in different areas in power systems and power electronics [24]–[27]. The important difference of DPM with conventional phasor analysis is in considering the time derivative of the phasors. Therefore, DPM can represent the fast electromagnetic dynamics of a network more precisely. In the following section, DPM for a simple two-node power system is presented.

A. Dynamic Phasor Model of a Two-Node System

Consider a simple two-node system shown in Fig. 1. Active and reactive powers injected from the first bus of this system can be defined as [26]:

$$\begin{aligned} P &= \frac{Ls+R}{|Z_e|^2}(V_1^2 - V_1V_2\cos\Phi_{V_1}) + \frac{X_L}{|Z_e|^2}(V_1V_2\sin\Phi_{V_1}) \\ Q &= \frac{X_L}{|Z_e|^2}(V_1^2 - V_1V_2\cos\Phi_{V_1}) - \frac{Ls+R}{|Z_e|^2}(V_1V_2\sin\Phi_{V_1}) \end{aligned} \tag{7}$$

where $X_L := L(2\pi f_n)$, $|Z_e| := \sqrt{(Ls+R)^2 + X_L^2}$. It is assumed that bus number 2 is considered as the reference for angle, which means $\Phi_{V_2} = 0$. By linearizing (7) around the equilibrium voltage V_{1_e}, the transfer function between active and reactive power deviations and local frequency and voltage deviations, can be written as:

$$\begin{bmatrix} P \\ Q \end{bmatrix} = \begin{bmatrix} \frac{X_L V_{1_e}^2}{s|Z_e|^2} & \frac{(Ls+R)V_{1_e}}{|Z_e|^2} \\ -\frac{(Ls+R)V_{1_e}^2}{s|Z_e|^2} & \frac{X_L V_{1_e}}{|Z_e|^2} \end{bmatrix} \begin{bmatrix} f \\ V \end{bmatrix} \tag{8}$$

In conventional power system analysis, the impact of Ls is usually ignored, which leads to inaccurate electromagnetic transient dynamics. Furthermore, in distribution grids, the value of R is not negligible, thus the system is coupled.

B. Input/Output Definition for Microgrid

As a general case, assume a power system including κ DGs and ℓ loads. The vector of desired active power of all DGs can be defined as $\bar{P}_{DG} := [\bar{p}_1, \ldots, \bar{p}_\kappa]^\mathsf{T}$. The vector of measured active power of DGs (i.e. P_{DG}) is defined similarly. The active power error vector can be defined as $P_e = \bar{P}_{DG} - P_{DG}$. With similar convention, vector of desired reactive power (i.e. $\bar{Q}_{DG}$), vector of measured reactive power (i.e. Q_{DG}), vector of reactive power error (i.e. Q_e), vector of desired frequency (i.e. $\bar{f}_{DG}$) and vector of desired voltage (i.e. $\bar{V}_{DG}$) of DGs can be defined. The vector of active power of loads is defined as $P_L := [p_{L_1}, \ldots, p_{L_\ell}]^\mathsf{T}$ and similarly the vector of load reactive power (i.e. $\bar{Q}_L$) can be defined. Accordingly, the input/output relation of the MIMO plant corresponding to the power system (G_{comp} in Fig. 2) can be written as:

$$[P_{DG}^\mathsf{T}, Q_{DG}^\mathsf{T}]^\mathsf{T} - [P_d^\mathsf{T}, Q_d^\mathsf{T}]^\mathsf{T} = G_{\text{comp}}[\bar{f}_{DG}^\mathsf{T}, \bar{V}_{DG}^\mathsf{T}]^\mathsf{T} \tag{9}$$

where $[P_d^\mathsf{T}, Q_d^\mathsf{T}]^\mathsf{T}$ is output power disturbance vector. Using DPM, the complete model of the grid including line power flow and the elements in the grid such as VSI and the SG is proposed in [28]. The block diagram of a general microgrid is depicted in Fig. 2 and its parameters are explained in Table I.

C. Proposed Controller Design Method

The design method includes the following steps:

1) Performance in Disturbance Rejection: To reduce the impact of disturbances, the weighted 2-norm of the output sensitivity function $\mathcal{S} = (I + G_{\text{comp}}K)^{-1}$ can be minimized:

$$\min_K \|W_1\mathcal{S}\|_2 \tag{10}$$

where W_1 is the output sensitivity weighting filter. Since the disturbances in power systems are mostly in the form of connection or disconnection of the loads, the step response of sensitivity function has high importance. Consequently, considering the relation of 2-norm in time-domain and frequency-domain, the 2-norm of low-pass filtered sensitivity function is minimized in order to reduce the time-domain oscillation generated by low-frequency disturbances.

2) Active Power-Sharing: Proportional active power-sharing can be achieved by investigating the sub-matrix of sensitivity function which relates the active power error to active power disturbance. This disturbance is the impact of the changes in active power loads on the drawn power at the DG bus. The sensitivity function $\mathcal{S}$ is split into 4 parts:

$$\begin{bmatrix} P_e \\ Q_e \end{bmatrix} = \begin{bmatrix} S_{11} & S_{12} \\ S_{21} & S_{22} \end{bmatrix} \begin{bmatrix} P_d \\ Q_d \end{bmatrix} \tag{11}$$

S_{11} defined above is the transfer function of active power disturbance to active power tracking error. For example, assume an active power disturbance p_{d_i} is applied to DG node i:

$$P_e = S_{11}\left[\ \ldots, p_{d_i}, \ldots\ \right]^\mathsf{T} \tag{12}$$

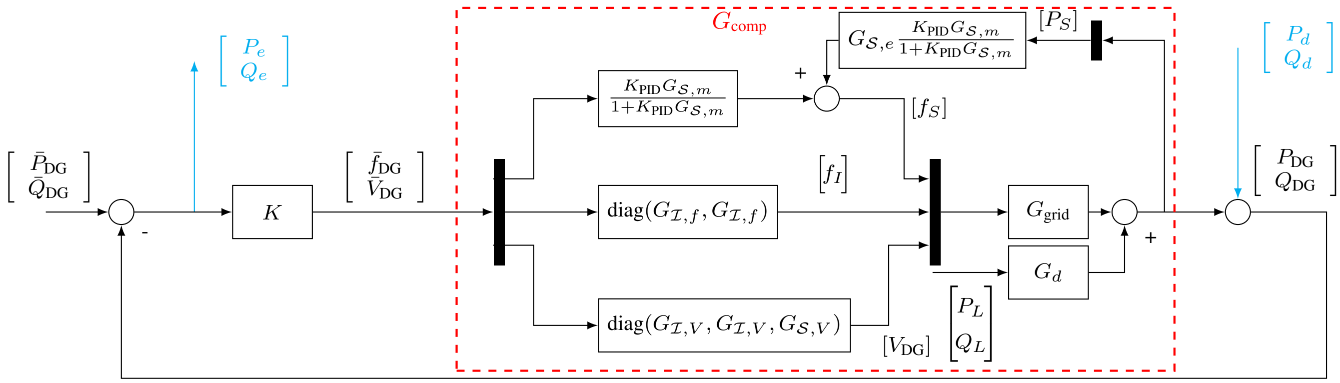

Fig. 2. Block diagram of complete model of the power system

Then, if power is shared proportionally, the following steady-state tracking errors should be obtained:

$$p_{e_j} = \frac{p_{n_j}}{p_{\text{tot}}} p_{d_i} \text{ for } j = 1, \ldots, \kappa \tag{13}$$

where p_{n_j} is the nominal power of the j-th DG unit and $p_{\text{tot}} = p_{n_1} + \cdots + p_{n_\kappa}$. The same relation should also hold for the other disturbances, which means $S_{11}(j\omega)|_{\omega=0}$ should take the following value:

$$S_{11}^0 = \frac{1}{p_{\text{tot}}} \begin{bmatrix} p_{n_1} & \cdots & p_{n_1} \\ \vdots & \ddots & \vdots \\ p_{n_\kappa} & \cdots & p_{n_\kappa} \end{bmatrix} \tag{14}$$

This leads to the following constraint:

$$S_{11}(j\omega)|_{\omega=0} = S_{11}^0 \tag{15}$$

According to (11) and (15), S_{11} is needed for power-sharing. To formulate the constraints in form of (3), the following transformation can be applied to $\mathcal{S}$:

$$[S_{11} \quad \sigma S_{12}] = \underbrace{\begin{bmatrix} I & 0 \end{bmatrix}}_{W_L} \mathcal{S} \underbrace{\text{diag}\,(I, \sigma I)}_{W_R} \tag{16}$$

where $\sigma \in \mathbb{R}$ is a small number to make W_R invertible. Using this transformation

$$\|W_L \mathcal{S} W_R\|_2^2 = \|S_{11}\|_2^2 + \sigma^2 \|S_{12}\| \approx \|S_{11}\|_2^2 \tag{17}$$

As the power-sharing problem is focused on steady-state, the first frequency is the most important point. Consequently, the problem of power-sharing can be written as:

$$\min_K \left\| W_{L1} \mathcal{S}_1 W_{R1} - [S_{11}^0 \quad 0] \right\|_2 \tag{18}$$

3) Frequency and Voltage Performance: Usually when the loads or the references for DG power change, voltage and frequency of the system deviate from the nominal values. To minimize the deviation in frequency and voltage as well as the frequency steady-state error, weighted 2-norm of the input sensitivity function $\mathcal{U} = K(I + G_{\text{comp}} K)^{-1}$ can be minimized.

$$\min_K \|W_2 \mathcal{U}\|_2 \tag{19}$$

where W_2 is the input sensitivity weighting filter and the following relation holds for $\mathcal{U}$:

$$[\bar{f}_{\text{DG}}^{\mathsf{T}}, \bar{V}_{\text{DG}}^{\mathsf{T}}]^{\mathsf{T}} = \mathcal{U}(j\omega)[P_d^{\mathsf{T}}, Q_d^{\mathsf{T}}]^{\mathsf{T}} \tag{20}$$

In general, at each frequency point, a higher weight will result in a lower deviation. Particularly, in order to reduce the frequency steady-state error W_2 should have high gain at low frequencies.

4) Complete Design Problem: Combining the mentioned specifications leads to the following multi-objective optimization problem:

$$\begin{aligned} \min_K \quad & \underbrace{\|W_1 \mathcal{S}\|_2}_{\text{Disturbance Rejection}} + \underbrace{\|W_2 \mathcal{U}\|_2}_{\text{Freq./Volt. Performance}} \\ \text{s.t.} \quad & S_{11}(j\omega_k)|_{k=1} = S_{11}^0 \qquad \text{(Power-Sharing)} \end{aligned} \tag{21}$$

Then, using the convex formulation from (6), the robust control design problem in (21) can be written as a convex optimization problem with LMI constraints:

$$\begin{aligned} &\min \quad \underbrace{\alpha\, \text{tr}(\Gamma_{P1})}_{\text{Power-Sharing}} + \sum_{k=1}^{N} \left[\underbrace{\text{tr}(\Gamma_{Sk})}_{\text{Dist. Rej.}} + \underbrace{\text{tr}(\Gamma_{Uk})}_{\text{Freq./Volt. Perf.}} \right] \\ &\begin{bmatrix} \Gamma_{Sk} & W_{1k} Y \\ (W_{1k} Y_k)^* & M_k^* M_{ck} + M_{ck}^* M_k - M_{ck}^* M_{ck} \end{bmatrix} > 0, \\ &\begin{bmatrix} \Gamma_{Uk} & W_{2k} X_k \\ (W_{2k} X_k)^* & M_k^* M_{ck} + M_{ck}^* M_k - M_{ck}^* M_{ck} \end{bmatrix} > 0, \\ &\begin{bmatrix} \Gamma_{P1} & B \\ B^* & \mathbf{M}_{W1} \end{bmatrix} > 0 \\ &Y_k^* Y_{ck} + Y_{ck}^* Y_k - Y_{ck}^* Y_{ck} > 0, \end{aligned} \tag{22}$$

for all $k = 1, \ldots, N$, where $B = W_{L1} Y_1 - [S_{11}^0 \quad 0] W_{R1}^{-1} M_1$. The scalar α is a weighting factor that denotes the importance of the power-sharing, and $\Gamma_{Sk} > 0$, $\Gamma_{Uk} > 0$ are auxiliary positive definite matrix variables as defined for the output and input sensitivity functions corresponding to k^{th} frequency point, respectively. In the same way, $\Gamma_{P1} > 0$ is the auxiliary positive definite matrix variable defined for the power-sharing at steady-state (ω_1). The necessary and sufficient condition for the first stability constraint (i.e. $\det(Y) \neq 0$, $\forall \omega \in \Omega$) is $Y^* Y > 0$. Since this constraint is not convex, it can be linearized around the initial controller as $Y_c^* Y + Y^* Y_c - Y_c^* Y_c > 0$. The last constraint in (22) is added to satisfy this constraint for all frequencies. Since the problem is an approximation of the original non-convex problem, the obtained solution depends on the initial controller. Therefore, an iterative approach is used, where the optimization problem is solved multiple times using the calculated controller K of the previous step as the new initial controller K_c. This choice always guarantees closed-loop stability (assuming the initial choice of K_c is stabilizing). Since the objective function is non-negative and non-increasing, the iteration converges to a locally optimal solution of the original non-convex problem.

It can be shown that for each stable plant one choice for stabilizing initial controller is $K_c = \epsilon I$ provided that ϵ is sufficiently small. In order to satisfy the third condition of stability, the initial controller matrices can be selected as:

$$X_c = \epsilon z^{\delta} \ , \ Y_c = I z^{\delta}$$

It should be mentioned that for selecting the order (i.e. δ) in designing the controller, the order of the controller is set to a very low value (say 2 or 3) initially. If the performance using this order is not satisfactory, the order is increased by one and the design procedure is reiterated.

5) Communication Graph: The controller design method proposed in this paper is capable of handling different structure of communication systems by choosing centralized, distributed or decentralized controller structure. If there is no data communication between two nodes, the corresponding elements will be substituted by zero in X matrix. As an illustrative example, consider a microgrid with three DGs (DG_1, DG_2, DG_3). Controller of each DG calculates its command signals based on the local measurements and measurements transmitted from other DGs. Assume that the available infrastructure provides communication links DG_1-DG_2 and DG_2-DG_3 but no communication link between DG_1 and DG_3. Therefore the following structure should be considered for $\underline{X}_i$ for $i \in \{1, 2, \cdots, \delta\}$:

$$\begin{array}{cc} & \begin{array}{cc} \text{Local} & \text{Distributed} \end{array} \\ \underline{X}_i = & \begin{bmatrix} x_i^{1,1} & x_i^{1,2} & x_i^{1,3} & x_i^{1,4} & 0 & 0 \\ x_i^{2,1} & x_i^{2,2} & x_i^{2,3} & x_i^{2,4} & 0 & 0 \\ x_i^{3,1} & x_i^{3,2} & x_i^{3,3} & x_i^{3,4} & x_i^{3,5} & x_i^{3,6} \\ x_i^{4,1} & x_i^{4,2} & x_i^{4,3} & x_i^{4,4} & x_i^{4,5} & x_i^{4,6} \\ 0 & 0 & x_i^{5,3} & x_i^{5,4} & x_i^{5,5} & x_i^{5,6} \\ 0 & 0 & x_i^{6,3} & x_i^{6,4} & x_i^{6,5} & x_i^{6,6} \end{bmatrix} \end{array} \tag{23}$$

6) Communication Delay: The proposed method is capable of considering communication delay in controller design by defining it as a fixed term in the controller. Assume that there is d-sampling time delay for data transmission from node i to node j. Then, by multiplying both (i, j)-th and (j, i)-th element of F_X by z^{-d}, the impact of communication delay can be considered in the controller design. In order to clarify the idea, in the above-mentioned illustrative example, assume that each communication link has d samples delay. This delay can be included in the fixed term of the controller as follows:

$$F_X(z) = \begin{bmatrix} \mathbf{1}_{2\times2} & z^{-d}\mathbf{1}_{2\times2} & \mathbf{0}_{2\times2} \\ z^{-d}\mathbf{1}_{2\times2} & \mathbf{1}_{2\times2} & z^{-d}\mathbf{1}_{2\times2} \\ \mathbf{0}_{2\times2} & z^{-d}\mathbf{1}_{2\times2} & \mathbf{1}_{2\times2} \end{bmatrix} \tag{24}$$

TABLE II
LINE PARAMETERS

Line	R [Ω]	X [Ω]	Line	R [Ω]	X [Ω]
1 - 2	0.018	0.0034	4 - 8	0.09	0.017
1 - 3	0.018	0.0034	8 - 9	0.045	0.0085
2 - 7	0.15	0.11	5 - 6	0.09	0.017
2 - 10	0.3	0.22	6 - 7	0.3	0.22
3 - 4	0.45	0.085	9 - 10	0.3	0.22
3 - 5	0.3	0.22			

TABLE III
DG UNITS PARAMETERS

BESS	
Bus:	[8, 10]
Output filter Parameters:	R_t = 10mΩ, L_t = 450 μH
	R_g = 58mΩ, L_g = 420 μH, C_f = 50 μF
Time Constants:	$\tau_\omega = 5 \cdot 10^{-4}$, $\tau_U = 5 \cdot 10^{-4}$
Nom. apparent power:	[70, 40] KVA
Synchronous Generator	
Bus:	[5]
Inertia Constant:	H = 1.5
Internal Impedance:	R_o = 19mΩ, L_o = 2.7 mH
Time Constants:	$\tau_m = 0.1$, $\tau_U = 0.05$
Speed Controller:	k_p = 3.18, k_i = 4.77, k_d=0.8, T_f = 0.05
Nom. apparent power:	70 KVA
Inverter	
Bus:	[1,2,7,8,10]
parameters:	Switching Freq.: 6.25 KHz, DC Voltage: 500 V
PV	
Bus:	[1, 2, 7]
Output filter Parameters:	R_t = 10mΩ, L_t = 450 μH
	R_g = 58mΩ, L_g = 420 μH, C_f = 50 μF
Active Power:	10 kW
Loads	
Bus:	[3, 4, 6, 9]
Active/Reactive Power:	[30, 20, 25, 45] kW / [0, 0, 0, 0] VAr

IV. CASE STUDY

The proposed method is applied to a microgrid illustrated in Fig. 3, which is a 50 Hz/230 V islanded grid including two VSI-interfaced Battery Energy Storage Systems (BESSs), one SG, three PV units in current-controlled mode and four constant-power loads. The lines are either resistive with X/R-ratio of 0.18 or mixed with X/R-ratio close to 1. Furthermore, each VSI is filtered with an LCL-type output filter. The SG is operated in speed control mode and is equipped with an internal speed controller. The parameters of lines and DGs are given in Table II and Table III, respectively.

A. Frequency Response Function

In this paper, the measurement data is provided through numerical real-time simulation of the grid including the switching inverters. To simplify the design, all controller inputs and outputs are assumed to be normalized to per unit with $V_{\text{base}} = 325\ V (= 230\sqrt{2})$, $f_{\text{base}} = 50$ Hz, $S_{\text{base}} = 100$ kVA. In the operating point, DGs are working in 50 percent of their nominal powers. A Pseudo-Random Binary Sequence (PRBS) signal with small magnitude is added to the closed-loop system references (i.e. $[\bar{P}_{DG}, \bar{Q}_{DG}]^\mathsf{T}$) while operating in normal condition and the output of the plant (i.e. $[P_{DG}, Q_{DG}]^\mathsf{T}$) are measured. Ten periods of an 8-order PRBS with a sampling time of 5 ms and a magnitude of 0.05 p.u. is applied. The last three periods of the excitation signal added to the reference of the active power of SG and the actual power injected to the grid at bus No. 5 are shown in Fig. 4.

The frequency response of the closed-loop transfer function $\mathcal{T} = G_{\text{comp}} K (I + G_{\text{comp}} K)^{-1}$ can be computed using Fourier

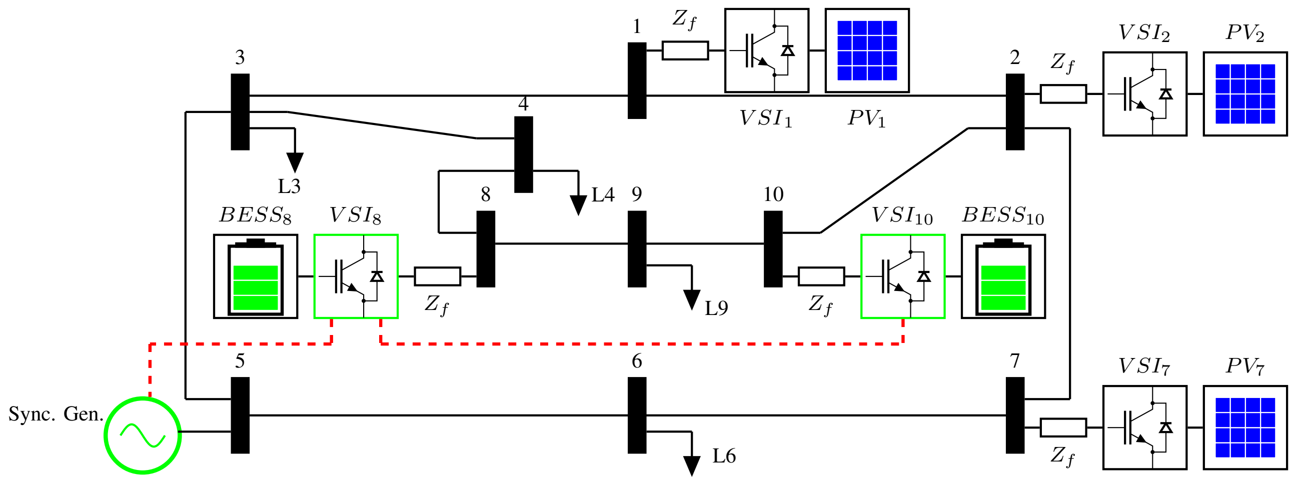

Fig. 3. Single-line diagram of microgrid (solid line: power line, dashed line: communication, L_i: load number i, Z_f: LCL filter)

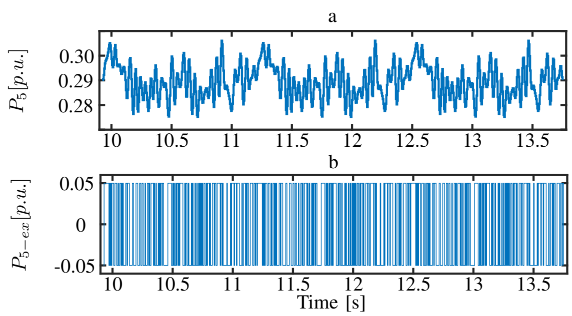

Fig. 4. a) Output power at bus No 5, b) Excitation added to ref. of SG

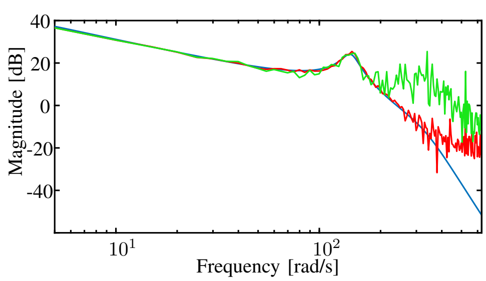

Fig. 5. Frequency response of the active power at bus No. 5 to the frequency reference of the SG at bus No. 5 with linear inverters (red), switching inverters (green) and the linearized parametric model using DPM (blue)

transform of input and output data. Then G_{comp} can be calculated as

$$G_{\text{comp}}(j\omega_k) = \mathcal{T}(j\omega_k)(K(j\omega_k)(I - T(j\omega_k)))^{-1}$$

The results of frequency response calculated using the measurement data are compared with parametric DPM. As an example, the response of active power injected to bus number 5 to the frequency reference of the SG is shown in Fig. 5

B. Controller Design

An 8-th order controller is designed for the grid in Fig. 3 by solving the convex optimization problem given in (22). For this example, $\epsilon = 0.01$ is sufficiently small to achieve the desired performance while avoiding numerical problems. The weighting factor α is chosen to be 1000. The weighting filters are chosen as $W_1^{-1} = 1.3s/(250+s)I$ and $W_2^{-1} = \beta I$ where $\beta = 0.01$ for $\omega < 100$ rad/s and $\beta = 0.1$ for $\omega > 100$ rad/s. Two sampling delays are considered for data transmission between K_8 and K_{10}. The optimization problem is then formulated in Matlab using Yalmip [29] and solved using Mosek [30]. The whole procedure of experiment (using power system measurement of the real-time simulation), frequency response calculation and controller design (using a desktop computer) take less than 3 minutes for this example.

C. Hardware-In-the-Loop validation

To validate the performance of the obtained controller, the grid shown in Fig. 3 is simulated in HIL setup including an Opal-rt real-time simulator and MyRIO controllers provided by National Instruments. In contrast with most of validations in the literature, which use simplified average models, the inverters of the batteries are simulated as the switching elements which inject harmonics to the system. The controller for inverters in bus No. 8 (K_8) and bus No. 10 (K_{10}) are separately implemented on two MyRIOs coded by LABVIEW as distributed controllers. Two communication types are employed in this HIL setup:

1) Sharing the data between K_8 and K_{10} using User Datagram Protocol (UDP) on WiFi with no guarantee for safe transmission of the data, which is the case when the available communication resources are limited in the actual implementation.
2) Sending the local measurement values calculated in Opal-rt real-time simulator to the controller using the analog noisy signals.

Moreover, to have a realistic experimental result, no synchronization signal between opal and two controllers are employed. This results in asynchronous operation of two controllers, which is the case in actual power systems.

The results of the proposed Data-driven Distributed Primary Secondary (DDPS) controller, the classical droop controller

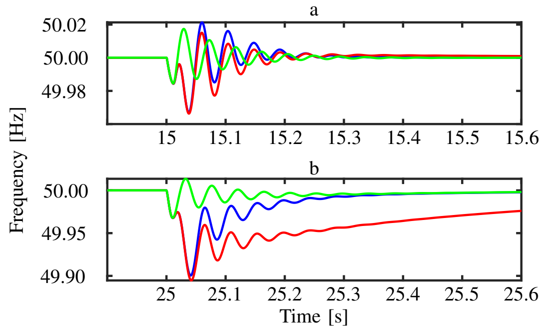

Fig. 6. SG frequency using different methods in a) impulse and b) step disturbance (red: droop with a central integrator, blue: DAPI, green: DDPS)

TABLE IV
FREQUENCY CONTROL COMPARISON

Method	Frequency nadir [mHz]	Settling time*[ms]
Droop	106	690
DAPI	100	181
DDPS	34	17

* The settling time is defined as the time that the frequency has less than 20 mHz frequency drop after addition of load and stays in that condition.

with centralized secondary control, and droop controller with a Distributed Averaging PI (DAPI) [7] are compared. In this experiment, a load with double size of L_4 has been connected at t=15 s for 0.01s at bus number 4 to show the impact of impulsive loads and L_6 is stepped up from 25 kW to 45 kW at t = 25 s to show steady-state disturbance damping. In Fig. 6, the instantaneous frequency at SG bus after the impulsive and step load is shown. It can be seen that with droop and DAPI controllers, the SG frequency experiences significant oscillations and it takes a long time until the nominal frequency is recovered. The results have been summarized in Table IV. The controller designed in this paper is able to reduce the frequency nadir and its settling time considerably.

The frequency at bus No. 8 and 10, where the BESSs are located, achieved by droop controller, DAPI controller, and controller designed by the proposed method have been shown in Fig. 7 and Fig. 8, respectively. It can be observed that the frequency with the proposed controller has a very low sensitivity to disturbances in comparison to other methods. Since there is no decoupling, both frequency and voltage contribute to disturbance rejection which results in less frequency oscillation at VSI nodes. The superiority of considering the couplings in controller design and also taking advantage of the independence of VSI frequency from physical states can be seen obviously by applying the proposed method.

Fig. 9 shows the active output power of the DGs and proportional power-sharing.

The voltage magnitude at a PV, Battery and SG buses using different methods are compared in Fig. 10 and their normalized two-norm are compared in Table V, which shows improvement

TABLE V
2-NORM OF VOLTAGE DEVIATION AT DIFFERENT BUSES

	bus #2	bus #5	bus #8
Droop	6.60	6.62	4.69
DAPI	6.64	6.61	4.69
DDPS	5.60	5.84	3.92

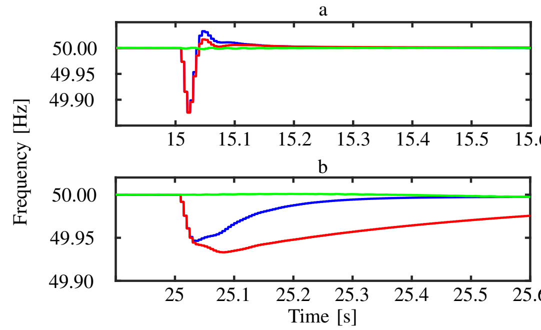

Fig. 7. VSI$_8$ frequency applying different methods in a) impulse and b) step disturbance (red: droop with central integrator, blue: DAPI, green: DDPS)

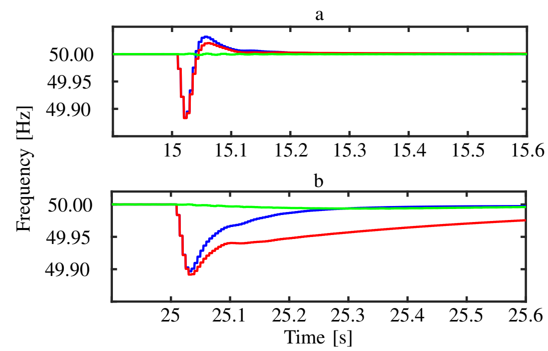

Fig. 8. VSI$_{10}$ frequency applying different methods in a) impulse and b) step disturbance (red: droop with central integrator, blue: DAPI, green: DDPS)

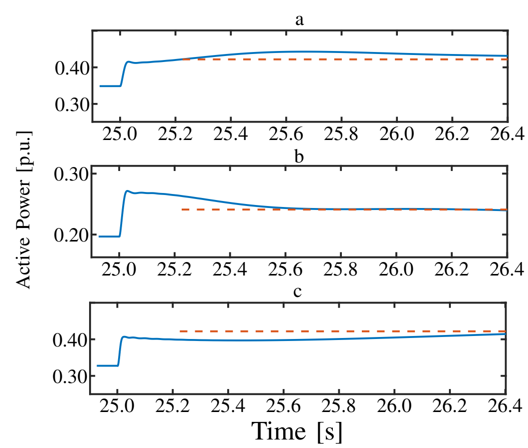

Fig. 9. Active power-sharing using DDPS a) VSI_8, b) VSI_{10}, c) SG (solid line: active power, dashed line: the proportionally shared active power)

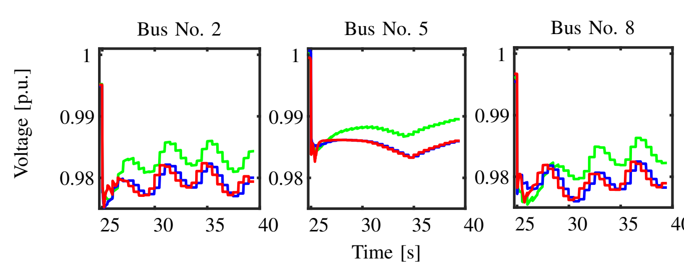

Fig. 10. Bus voltages applying different methods in a) impulse and b) step disturbance (red: droop with central integrator, blue: DAPI, green: DDPS)

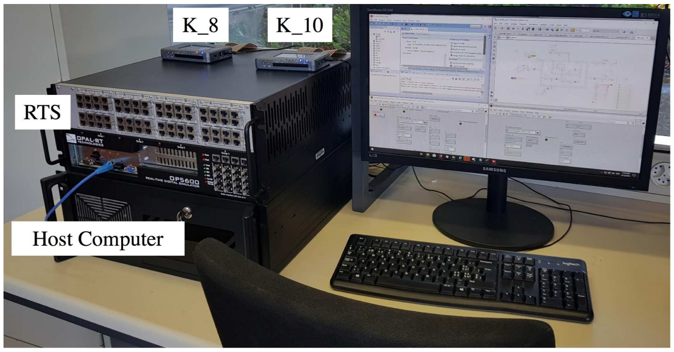

Fig. 11. HIL setup

in voltage recovery.

V. Conclusion

It has been shown how the problem of primary and secondary control design for islanded microgrids including both VSI and SG can be expressed in a H_2 framework. The proposed method directly uses the measurement data with no need for a parametric model of the system. Expressing desired performance specifications as convex constraints on sensitivity functions makes it possible to apply a convex optimization method to design the controller parameters. This results in a systematic design approach that guarantees robust stability and allows the realization of different performance objectives such as good transient performance and proportional power sharing. HIL results show that significant superior performance can be achieved as compared to classical hierarchical droop approaches. As a future work, non-linearities of the system can be considered as either frequency domain or multi-model uncertainty, which can be extracted using the measurement data in different operating points.

References

[1] D. E. Olivares, A. Mehrizi-Sani, A. H. Etemadi, C. A. Cañizares, R. Iravani, M. Kazerani, A. H. Hajimiragha, O. Gomis-Bellmunt, M. Saeedifard, R. Palma-Behnke *et al.*, "Trends in microgrid control," *IEEE Trans. Smart Grid*, vol. 5, no. 4, pp. 1905–1919, 2014.

[2] M. C. Chandorkar, D. M. Divan, and R. Adapa, "Control of parallel connected inverters in standalone ac supply systems," *IEEE Transactions on Industry Applications*, vol. 29, no. 1, pp. 136–143, Jan 1993.

[3] J. M. Guerrero, J. C. Vasquez, J. Matas, L. G. De Vicuña, and M. Castilla, "Hierarchical control of droop-controlled AC and DC microgridsa general approach toward standardization," *IEEE Trans. Ind. Electron.*, vol. 58, no. 1, pp. 158–172, 2011.

[4] A. Bidram and A. Davoudi, "Hierarchical structure of microgrids control system," *IEEE Trans. Smart Grid*, vol. 3, no. 4, pp. 1963–1976, Dec 2012.

[5] A. Mehrizi-Sani and R. Iravani, "Potential-function based control of a microgrid in islanded and grid-connected modes," *IEEE Trans. Power Syst.*, vol. 25, no. 4, pp. 1883–1891, Nov 2010.

[6] F. Guo, C. Wen, J. Mao, and Y.-D. Song, "Distributed secondary voltage and frequency restoration control of droop-controlled inverter-based microgrids," *IEEE Trans. Ind. Electron.*, vol. 62, no. 7, pp. 4355–4364, 2015.

[7] J. W. Simpson-Porco, F. Dörfler, and F. Bullo, "Synchronization and power sharing for droop-controlled inverters in islanded microgrids," *Automatica*, vol. 49, no. 9, pp. 2603–2611, 2013.

[8] M. N. Marwali, J. Jung, and A. Keyhani, "Stability analysis of load sharing control for distributed generation systems," *IEEE Trans. Energy Convers.*, vol. 22, no. 3, pp. 737–745, Sep. 2007.

[9] Y. A. I. Mohamed and E. F. El-Saadany, "Adaptive decentralized droop controller to preserve power sharing stability of paralleled inverters in distributed generation microgrids," *IEEE Trans. Power Electron.*, vol. 23, no. 6, pp. 2806–2816, Nov 2008.

[10] C. Y. Chang and W. Zhang, "Distributed control of inverter-based lossy microgrids for power sharing and frequency regulation under voltage constraints," *Automatica*, vol. 66, pp. 85–95, 2016.

[11] J. Schiffer, R. Ortega, A. Astolfi, J. Raisch, and T. Sezi, "Conditions for stability of droop-controlled inverter-based microgrids," *Automatica*, vol. 50, no. 10, pp. 2457–2469, 2014.

[12] N. Ainsworth and S. Grijalva, "A structure-preserving model and sufficient condition for frequency synchronization of lossless droop inverter-based ac networks," *IEEE Trans. Power Syst.*, vol. 28, no. 4, pp. 4310–4319, Nov 2013.

[13] Q.-C. Zhong and G. Weiss, "Synchronverters: Inverters that mimic synchronous generators," *IEEE Trans. Ind. Electron.*, vol. 58, no. 4, pp. 1259–1267, 2011.

[14] N. Soni, S. Doolla, and M. C. Chandorkar, "Improvement of transient response in microgrids using virtual inertia," *IEEE Trans. Power Del.*, vol. 28, no. 3, pp. 1830–1838, 2013.

[15] B. K. Poolla, S. Bolognani, and F. Dorfler, "Optimal placement of virtual inertia in power grids," *IEEE Trans. Autom. Control*, vol. 62, no. 12, pp. 6209–6220, 2017.

[16] M. Hossain, H. R. Pota, M. A. Mahmud, and M. Aldeen, "Robust control for power sharing in microgrids with low-inertia wind and PV generators," *IEEE Trans. Sustain. Energy*, vol. 6, no. 3, pp. 1067–1077, 2015.

[17] J. W. Simpson-Porco, F. Dorfler, and F. Bullor, "Voltage stabilization in microgrids via quadratic droop control," *IEEE Trans. Autom. Control*, vol. 62, no. 3, pp. 1239–1253, 2017.

[18] Q. L. Lam, A. I. Bratcu, D. Riu, and J. Mongkoltanatas, "Multi-variable H-infinity robust control applied to primary frequency regulation in microgrids with large integration of photovoltaic energy source," in *Industrial Technology (ICIT), 2015 IEEE International Conference on*. IEEE, 2015, pp. 2921–2928.

[19] H. Bevrani, M. R. Feizi, and S. Ataee, "Robust frequency control in an islanded microgrid: H_∞ and μ-synthesis approaches," *IEEE Trans. Smart Grid*, vol. 7, no. 2, pp. 706–717, 2016.

[20] M. S. Sadabadi, A. Karimi, and H. Karimi, "Fixed-order decentralized/distributed control of islanded inverter-interfaced microgrids," *Control Engineering Practice*, vol. 45, pp. 174–193, 2015.

[21] M. S. Sadabadi, Q. Shafiee, and A. Karimi, "Plug-and-play voltage stabilization in inverter-interfaced microgrids via a robust control strategy," *IEEE Trans. Control Syst. Technol.*, vol. 25, no. 3, pp. 781–791, 2017.

[22] A. Karimi and C. Kammer, "A data-driven approach to robust control of multivariable systems by convex optimization," *Automatica*, vol. 85, pp. 227–233, 2017.

[23] S. R. Sanders, J. M. Noworolski, X. Z. Liu, and G. C. Verghese, "Generalized averaging method for power conversion circuits," *IEEE Trans. Power Electron.*, vol. 6, no. 2, pp. 251–259, April 1991.

[24] K. De Brabandere, B. Bolsens, J. Van Den Keybus, J. Driesen, M. Prodanovic, and R. Belmans, "Small-signal stability of grids with distributed low-inertia generators taking into account line phasor dynamics," in *Electricity Distribution, 2005. CIRED 2005. 18th International Conference and Exhibition on*. IET, 2005, pp. 1–5.

[25] M. C. Chudasama and A. M. Kulkarni, "Dynamic phasor analysis of ssr mitigation schemes based on passive phase imbalance," *IEEE Trans. Power Syst.*, vol. 26, no. 3, pp. 1668–1676, Aug 2011.

[26] X. Guo, Z. Lu, B. Wang, X. Sun, L. Wang, and J. M. Guerrero, "Dynamic phasors-based modeling and stability analysis of droop-controlled inverters for microgrid applications," *IEEE Trans. Smart Grid*, vol. 5, no. 6, pp. 2980–2987, 2014.

[27] T. Yang, S. Bozhko, J. Le-Peuvedic, G. Asher, and C. I. Hill, "Dynamic phasor modeling of multi-generator variable frequency electrical power systems," *IEEE Trans. Power Syst.*, vol. 31, no. 1, pp. 563–571, Jan 2016.

[28] C. Kammer and A. Karimi, "Decentralized and distributed transient control for microgrids," *IEEE Trans. Control Syst. Technol.*, 2017.

[29] J. Löfberg, "YALMIP: A toolbox for modeling and optimization in MATLAB," in *CACSD Conference*, http://control.ee.ethz.ch/joloef/yalmip.php, 2004.

[30] MOSEK ApS, *The MOSEK optimization toolbox for MATLAB manual. Version 7.1*, 2015. [Online]. Available: http://docs.mosek.com/7.1/toolbox/index.html

APPENDIX B

Data-Driven LPV Controller Design for Islanded Microgrids

Published in the Proceedings of IFAC Symposium on System Identification (2021)

Accessible through this link: https://doi.org/10.1016/j.ifacol.2021.08.398

Data-Driven LPV Controller Design for Islanded Microgrids ⋆

Seyed Sohail Madani * **Alireza Karimi** *

* *Laboratoire d'Automatique, École Polytechnique Fédérale de Lausanne, 1015 Lausanne, Switzerland, (e-mail: {sohail.madani@epfl.ch, alireza.karimi@epfl.ch}).*

Abstract: This paper presents a data-driven multivariable Linear Parameter Varying (LPV) controller design method. The synthesis process is based on frequency-domain data corresponding to different operating points of the plant. The H_∞ performance and also stability constraints for frozen scheduling parameter are convexified around an initial stabilizing controller and solved using a convex optimization solver. This method has been applied to the combined primary and secondary controller design problem of electrical microgrids. The performance of the proposed method has been validated through simulating a microgrid including a synchronous generator, a battery storage and a photo-voltaic unit. The results show that using this method, high performance is achieved in different operating points.

Keywords: Data-driven, frequency control, linear parameter varying, power-sharing, microgrid control, distributed control.

1. INTRODUCTION

In model-based controller synthesis, the model is obtained either by first-principles approach or by parametric system identification. The former is prone to the uncertainty of the true physical parameters and unknown high order dynamics. The latter is basically a mapping from high dimensional space of data to low dimensional space of model parameters and needs an assumption on the structure of the model. In a data-driven approach, the measured data of the system can be used for controller synthesis bypassing the parametric identification step. Although the model-based methods are statistically more efficient when the model structure is known, the data-driven method may outperform the model-based methods in terms of control cost (see Formentin et al. (2014)) in the presence of unmodelled dynamics.

Data-driven methods can be categorized as time-domain and frequency-domain methods. The time-domain methods usually minimize a cost function which is a control performance defined in the time domain. Iterative Feedback Tuning (IFT) by Hjalmarsson et al. (1994), Virtual Reference Feedback Tuning (VRFT) by Campi et al. (2002), Correlation-based Tuning (nCbT) by van Heusden et al. (2011) and unfalsified control by Safonov and Tsao (1997) are some of the well-known methods in this category. Recently some new interests are observed for data-driven linear quadratic control in Berberich et al. (2019); Dai and Sznaier (2019); Goncalves Da Silva et al. (2019); Pang et al. (2019) and for data-driven model predictive control in Salvador et al. (2018); Coulson et al. (2018). Another group of data-driven methods define the constraints and objective function in the frequency domain (see Keel and Bhattacharyya (2008); Karimi and Galdos (2010); Karimi and Kammer (2017); Apkarian and Noll (2018); Kergus et al. (2019); van Solingen et al. (2018)) and use a finite number of the frequency-domain data to optimize the objective function by a convex or non-convex optimization method under constraints.

Although the model-based control of Linear Parameter Varying (LPV) systems has attracted the attention of researchers (e.g. Xie and Eisaka (2004) using Youla parameterization and see Hoffmann and Werner (2015) for a review), there is a limited number of data-driven LPV methods in the literature. A feed-forward precompensator using data-driven LPV method in a stochastic framework is proposed in Butcher and Karimi (2009). The LPV extensions of the VRFT method is proposed in Formentin and Savaresi (2011), where the controllers are linearly parameterized. This method is extended to the case where the structure of the controller is also learned from data using least-squares support vector machines in Formentin et al. (2016). The frequency-domain method in Karimi and Galdos (2010) is extended to LPV case and applied to a benchmark problem in Karimi and Emedi (2013). In this method, the controller is linearly parameterized and does not cover the MIMO case.

In this paper, a new data-driven LPV controller design method for multivariable systems represented by multiple sets of frequency-domain data in different operating points is proposed, which is a natural extension to the method proposed in Karimi and Kammer (2017). In this method, the controller is fully parameterized and all performance and stability constraints are written in the convex-concave

⋆ This project is carried out within the frame of the Swiss Centre for Competence in Energy Research on the Future Swiss Electrical Infrastructure (SCCER-FURIES) with the financial support of the Swiss Innovation Agency (Innosuisse - SCCER program). The work of S. S. Madani is supported by the Swiss National Science Foundation under Grant 200021_172828. *(Corresponding author: A. Karimi)*

form. Then, a convex optimization algorithm using Linear Matrix Inequalities (LMIs) is derived by linearization of the concave part around a stabilizing initial controller. The proposed method is applied to control of microgrids.

A microgrid (MG) can be defined as a small power system including different Distributed Generation units (DGs) and loads. MGs can be operated independently from the main grid which is called islanded mode. Power-sharing and voltage and frequency control in islanded MGs is a challenging nonlinear multivariable problem. A well-known category of MG control methods are model-free droop-based methods (see Chandorkar et al. (1993)), which are easy to design but have poor transient and steady-state performance without guarantee for stability. In contrast, the model-based methods either use high-order small-signal models linearized around an operating point (for example see Katiraei and Iravani (2006)) or non-linear static models ignoring the electromagnetic dynamics (e.g. Simpson-Porco et al. (2013); Schiffer et al. (2014); Ainsworth and Grijalva (2013); Chang and Zhang (2016)). The linear methods have stability and performance problems in other operating points and the nonlinear methods cannot guarantee good transient performance.

In this contribution, using the frequency-domain data of the system in different operating points, an LPV MIMO controller is designed for MGs, which includes power-sharing and frequency/voltage restoration. Because the original nonlinear system is represented only be a multiple set of data, the stability and performance are only guaranteed for the frozen scheduling parameters. However, it is a well-known fact that for systems with slow variation of scheduling parameter, it gives a good approximation of system in practice (see Shamma and Athans (1992)). MG control is a good example of this condition because the operating points (the scheduling parameters) are updated with a much higher sampling time than that of the feedback control loop (see Olivares et al. (2014)). Consequently, the assumption on the frozen scheduling parameter is valid and the closed-loop system remains stable in practice. The performance of the proposed method is validated through numerical simulation of an MG including a Synchronous Generator (SG), a Battery Energy Storage System (BESS) and a Photo-Voltaic (PV) unit.

The rest of the paper is organized as follows: In Section 2, the LPV controller design method is explained. Section 3 shows how the performance of an MG can be transformed into frequency-domain convex constraints and integrated into the proposed method. The case study results are given in Section 4 followed by some concluding remarks.

2. DATA-DRIVEN LPV CONTROLLER DESIGN

Assume the system to be controlled is an m-input, n-output system $\mathcal{G}(\theta)$, where $\theta \in \Theta$ is an exogenous vector of scheduling parameters of dimension n_θ and Θ is its range. This system, for any frozen vector of parameters θ, can be considered as a Multivariable Linear Time Invarient (MIMO-LTI) with frequency response $G(e^{j\omega},\theta) \in \mathbb{C}^{n\times m}$. It is assumed that $G(e^{j\omega},\theta)$ is bounded for all frequencies in $\omega \in \Omega$, where $\Omega = \left\{\omega \middle| -\frac{\pi}{T_s} \leq \omega \leq \frac{\pi}{T_s}\right\} \backslash B_g$, T_s is the sampling time of the control system and B_g corresponds to the poles of the plant on unit circle. In this paper, the discrete-time plant is considered, however, the formulation can be changed to continuous-time systems straightforwardly. Assume that $u(\kappa,\theta) \in \mathbb{R}^{m\times m}$ and $y(\kappa,\theta) \in \mathbb{R}^{n\times m}$ denotes the input and output of the plant at instant κ from m experiments, respectively. Also assume that N samples of noiseless input and output measurement are available and $u(\kappa,\theta) = 0$, $y(\kappa,\theta) = 0$ for $\kappa < 0$ and $\kappa > N$. Then, the corresponding plant frequency response based on the measurement data can be written as:

$$G(e^{j\omega},\theta) = \left[\sum_{\kappa=0}^{N-1} y(\kappa,\theta)e^{-j\omega T_s \kappa}\right]\left[\sum_{\kappa=0}^{N-1} u(\kappa,\theta)e^{-j\omega T_s \kappa}\right]^{-1} \tag{1}$$

For noisy and truncated data, the above relation gives an estimate of the frequency response of the system.

2.1 Controller Structure

Consider a vector $\rho(\theta)$ that includes all polynomial basis functions of $\theta = [\theta_1, \theta_2, \cdots, \theta_{n_\theta}]$ up to order α:

$$\begin{aligned}\rho(\theta) =&[\rho_1(\theta), \cdots, \rho_{n_\rho}(\theta)]\\ =&[\theta_1, \cdots, \theta_{n_\Theta}, \theta_1^2, \cdots, \theta_{n_\theta}^2, \cdots, \theta_1^\alpha, \cdots, \theta_{n_\Theta}^\alpha,\\ &\theta_1\theta_2, \theta_1\theta_3, \cdots, \theta_1^2\theta_2, \cdots, \theta_1\theta_2\theta_3, \cdots]\end{aligned} \tag{2}$$

Then, define the controller structure as:

$$K(z,\theta) = X(z,\theta)Y(z,\theta)^{-1} \tag{3}$$

where

$$\begin{aligned}X(z,\theta) = \big(&(\underline{X}_{0,0} + \underline{X}_{0,1}z + \cdots + \underline{X}_{0,\delta}z^\delta)+\\ &(\underline{X}_{1,0} + \underline{X}_{1,1}z + \cdots + \underline{X}_{1,\delta}z^\delta)\rho_1(\theta)+\\ &(\underline{X}_{2,0} + \underline{X}_{2,1}z + \cdots + \underline{X}_{2,\delta}z^\delta)\rho_2(\theta) + \cdots +\\ &(\underline{X}_{n_\rho,0} + \underline{X}_{n_\rho,1}z + \cdots + \underline{X}_{n_\rho,\delta}z^\delta)\rho_{n_\rho}(\theta)\big) \circ F_X(z,\theta)\end{aligned}$$

$$\begin{aligned}Y(z,\theta) = \big(&(\underline{Y}_{0,0} + \underline{Y}_{0,1}z + \cdots + \underline{Y}_{0,\delta-1}z^{\delta-1} + Iz^\delta)+\\ &(\underline{Y}_{1,0} + \cdots + \underline{Y}_{1,\delta-1}z^{\delta-1} + Iz^\delta)\rho_1(\theta)+\\ &(\underline{Y}_{2,0} + \cdots + \underline{Y}_{2,\delta-1}z^{\delta-1} + Iz^\delta)\rho_2(\theta) + \cdots +\\ &(\underline{Y}_{n_\rho,0} + \cdots + \underline{Y}_{n_\rho,\delta-1}z^{\delta-1} + Iz^\delta)\rho_{n_\rho}(\theta)\big) \circ F_Y(z,\theta)\end{aligned}$$

Note that $X(z,\theta)$ and $F_X(z,\theta)$ are $m\times n$ and $Y(z,\theta)$ and $F_Y(z,\theta)$ are $n\times n$ polynomial matrices and $\circ$ denotes the element-wise matrix multiplication. The controller parameters are $\underline{X}_{i,j} \in \mathbb{R}^{m\times n}$ and $\underline{Y}_{i,j} \in \mathbb{R}^{n\times n}$. The controller fixed terms are defined in $F_X(z,\theta)$ and $F_Y(z,\theta)$. It is assumed that for all $\theta \in \Theta$, an initial stabilizing controller $K_c(z,\theta) = X_c(z,\theta)Y_c(z,\theta)^{-1}$ is available. Note that it is not a restrictive assumption in practice. In general, if the plant is stable, a controller with a sufficiently small gain can stabilize the closed-loop system. For unstable plants, a stabilizing controller should be available for data acquisition that can be the initial controller. For the sake of simplicity in notation, the arguments related to frequency term and z are omitted in the rest of this paper.

2.2 Performance

Performance can be defined as H_∞, H_2 on closed-loop sensitivity functions. In the sequel, it is shown how H_∞ norm of weighted sensitivity functions can be minimized or considered as a constraint in a convex optimization problem using LMIs. Assume the following constraint:

$$\|W(\theta)\mathcal{U}(\theta)\|_\infty < 1, \quad \forall\theta \in \Theta \tag{4}$$

where $\mathcal{U}(\theta) = K(\theta)(I + L(\theta))^{-1}$ is the input sensitivity function and $L(\theta) = G(\theta)K(\theta)$. Although the weighting filters can be a function of θ, in the rest of the paper for the sake of simplicity, it is assumed that the filters are constant with respect to θ. If the system is closed-loop stable (will be discussed in the next part), the constraint in (4) can be written as:

$$(W\mathcal{U}(\theta))^* W\mathcal{U}(\theta) < I, \quad \forall\omega \in \Omega, \quad \forall\theta \in \Theta \tag{5}$$

where $(\cdot)^*$ denotes complex conjugate transpose. Using the definition of the input sensitivity function, the constraint in (5) can be written as:

$$(WK(\theta)(I + L(\theta))^{-1})^* WK(\theta)(I + L(\theta))^{-1} < I \tag{6}$$

for all $\omega \in \Omega$ and for all $\forall\theta \in \Theta$. Using (3), this constraint can be reformulated as:

$$(WX(\theta))^* WX(\theta) - Z(\theta)^* Z(\theta) < 0, \ \forall\omega \in \Omega, \forall\theta \in \Theta \tag{7}$$

where $Z(\theta) = Y(\theta) + G(\theta)X(\theta)$. Defining $Z_c(\theta) := Y_c(\theta) + G(\theta)X_c(\theta)$ and also considering the following inequality

$$Z(\theta)^* Z(\theta) \geq Z(\theta)^* Z_c(\theta) + Z_c(\theta)^* Z(\theta) - Z_c(\theta)^* Z_c(\theta),$$

constraint (7) can be convexified as follows:

$$(WX(\theta))^* WX(\theta) - \bar{Z}(\theta) < 0, \quad \forall\omega \in \Omega, \quad \forall\theta \in \Theta \tag{8}$$

where $\bar{Z}(\theta) := Z(\theta)^* Z_c(\theta) + Z_c(\theta)^* Z(\theta) - Z_c(\theta)^* Z_c(\theta)$. Using Schur complement lemma, this constraint can be written in LMI form as follows:

$$\begin{bmatrix} I & WX(\theta) \\ (WX(\theta))^* & \bar{Z}(\theta) \end{bmatrix} > 0, \quad \forall\omega \in \Omega, \quad \forall\theta \in \Theta \tag{9}$$

The controller performance can also be optimized by minimizing the infinity norm of the weighted output sensitivity function as follows:

$$\begin{aligned} &\min \gamma \\ \text{subject to:} \quad &\|W\mathcal{S}(\theta)\|_\infty < \gamma, \quad \forall\theta \in \Theta \end{aligned} \tag{10}$$

where $\mathcal{S}(\theta) = (I + L(\theta))^{-1}$ is the output sensitivity function. Given that the system is closed-loop stable, the constraint in (10) can be written as

$$(W\mathcal{S}(\theta))^* W\mathcal{S}(\theta) < \gamma I \quad \forall\omega \in \Omega, \ \forall\theta \in \Theta. \tag{11}$$

Similar to steps (6)-(9), for this constraint, a sufficient LMI can be written as follows:

$$\begin{bmatrix} \gamma I & WY(\theta) \\ (WY(\theta))^* & \bar{Z}(\theta) \end{bmatrix} > 0, \quad \forall\omega \in \Omega, \quad \forall\theta \in \Theta \tag{12}$$

2.3 Stability

It can be shown that controller $K(\theta) = X(\theta)Y(\theta)^{-1}$ stabilizes the plant $G(\theta)$ for a frozen θ given an initial stabilizing controller $K_c(\theta) = X_c(\theta)Y_c(\theta)^{-1}$ if and only if the following conditions hold:

(1) $\det(Y_c(\theta)) \neq 0$ for all $\omega \in \Omega$.
(2) $\det(Y(\theta)) \neq 0$ for all $\omega \in \Omega$.
(3) Initial controller and final controller share the same pole on unit circle.
(4) $Z(\theta)^* Z_c(\theta) + Z_c(\theta)^* Z(\theta) > 0$ for all $\omega \in \Omega$.
(5) Order of $\det(Y_c(\theta))$ equals order of $\det(Y(\theta))$.

For proof see Karimi and Kammer (2017). It can be shown that sufficient condition for the second condition is $\bar{Y}(\theta) > 0$ for all $\omega \in \Omega$ where

$$\bar{Y}(\theta) := Y(\theta)^* Y_c(\theta) + Y_c(\theta)^* Y(\theta) - Y_c(\theta)^* Y_c(\theta).$$

Moreover, it can be shown that sufficient condition for the forth condition is $\bar{Z}(\theta) > 0$ which is satisfied when (9) or constraint in (12) are satisfied for all $\omega \in \Omega$.

3. MICROGRID CONTROLLER DESIGN

Using Dynamic Phasor Model (DPM), the active power (P) and reactive power (Q) flow between nodes in the Laplace domain can be formulated as (see Guo et al. (2014)):

$$P = G_{pv}V + G_{pd}\Phi, \quad Q = G_{qv}V + G_{qd}\Phi \tag{13}$$

where V is the magnitude of dynamic phasor, Φ is the angle of dynamic phasor voltage, G_{pv}, G_{pd} are the transfer function between voltage and phase angle and active power, and G_{qv}, G_{qd} are the transfer function between voltage and phase angle and reactive power. The local frequency of bus voltage (i.e. f) can be defined as the derivative of the voltage angle. It should be noted that in this paper, f denotes the power signal frequency while ω denotes the frequency in which the Fourier transform of the signals is calculated. According to (13), a DG using its voltage and frequency can control active and reactive power. Assume the MG includs N_ℓ nodes having load and N_g nodes connected to DGs. The vectors of active and reactive powers of DGs are named as P and Q, respectively. The MG controller generates the reference for frequencies and voltages named respectively as f_g, V_g. Briefly, the inputs of the plant are $[f_g^\top, V_g^\top]^\top$ and the outputs are $[P^\top, Q^\top]^\top$.

3.1 Data-Driven Mircogrid Controller Design Problem

Assume that the closed-loop performance specifications are (I) providing power-sharing in steady-state, (II) limiting the oscillations in active and reactive powers, (III) limiting the oscillation in frequency and voltage, (IV) Rejecting load disturbance in steady-state in voltage and frequency, and, (V) providing stability guarantee. These specifications should be transformed into constraints on closed-loop sensitivity functions in order to be integrated into the controller design problem. Assume the objective is to define a constraint for the third and fourth specifications. Since voltage and frequency are the plant inputs, shaping the input sensitivity function can improve the performance of voltage and frequency. This constraint can be defined as:

$$\|W_2\mathcal{U}(\theta)\|_\infty < 1, \quad \forall\theta \in \Theta \tag{14}$$

where W_2 is the weighting filter for input sensitivity function. This constraint can be written as:

$$\begin{bmatrix} I & W_2X(\theta) \\ (W_2X(\theta))^* & \bar{Z}(\theta) \end{bmatrix} > 0, \quad \forall\omega \in \Omega, \quad \forall\theta \in \Theta \tag{15}$$

Having this constraint makes the problem a semi-infinite programming. In order to make the problem tractable, it can be changed to semi-definite programming by gridding over frequency and scheduling parameter. It should be noted that as an alternative to gridding, the scenario-based method could be used. Assume that the sets of gridded frequency and scheduling parameter are $\Omega_{N_\omega} = \{\omega_1, \omega_2, \ldots, \omega_{N_\omega}\}$ and $\Theta_{N_\theta} = \{\theta_1, \theta_2, \ldots, \theta_{N_\theta}\}$ where N_ω and N_θ are number of points in corresponding sets. Consequently, the constraint in (15) can be written as:

$$\begin{bmatrix} I & W_{2k}X_{k,i} \\ (W_{2k}X_{k,i})^* & \bar{Z}_{k,i} \end{bmatrix} > 0 \tag{16}$$

for $k = \{1, 2, \ldots, N_\omega\}$ and $i = \{1, 2, \ldots, N_\theta\}$ where $X_{k,i} := X(e^{j\omega_k}, \theta_i)$ and $W_{2k} := W_2(e^{j\omega_k})$ and the same convention holds for other variables. Since the active and reactive powers are the outputs of the plant, in order to meet the second specification, the transfer function of output sensitivity function should be shaped. This constraint can be defined as

$$\|W_1 \mathcal{S}(\theta)\|_\infty < 1 \tag{17}$$

where W_1 is the weighting filter for output sensitivity function. This constraint can be written as:

$$\begin{bmatrix} I & W_{1k}Y_{k,i} \\ (W_{1k}Y_{k,i})^* & \bar{Z}_{k,i} \end{bmatrix} > 0 \tag{18}$$

for $k = \{1, 2, \ldots, N_\omega\}$ and $i = \{1, 2, \ldots, N_\theta\}$.

Usually, in MGs, there is a high-level optimization-based controller, which calculates the references of DG active and reactive powers. This controller has a very large sampling time. However, between two updates of high-level reference commands, the loads change and this load should be shared between different generation units properly. A common way is to share power between generation units based on their nominal powers which is called proportional power-sharing. This requirement should be written as a constraint in frequency-domain to be integrated into controller design problem. The power-sharing can be seen as sharing the disturbance in terms of tracking error proportionally among DGs, which can be written as:

$$p_{e_j} = a_j p_{d_i} \tag{19}$$

for $j = 1, \ldots, N_g$ where p_{d_i}, p_{e_j} are disturbance at node $i \in \{1, \ldots, N_g\}$ and tracking error at bus j, respectively. Fixed sharing factor can be defined as $a_j = p_{n_j}/p_{\text{tot}}$ where p_{n_j} and p_{tot} are nominal power of DG at bus j and total nominal DG powers, respectively. Now, define P_d and P_e as the vector of active power disturbances and tracking error at DG buses, while similar definitions for reactive powers hold. According to the definition of $\mathcal{S}(\theta)$, it can be partitioned to four sub-matrices as:

$$\begin{bmatrix} P_e \\ Q_e \end{bmatrix} = \begin{bmatrix} \mathcal{S}_{\mathcal{PP}}(\theta) & \mathcal{S}_{\mathcal{PQ}}(\theta) \\ \mathcal{S}_{\mathcal{QP}}(\theta) & \mathcal{S}_{\mathcal{QQ}}(\theta) \end{bmatrix} \begin{bmatrix} P_d \\ Q_d \end{bmatrix} \tag{20}$$

Based on (19), it can be shown that steady-state proportional power-sharing condition is satisfied if:

$$\mathcal{S}_{\mathcal{PP}}(\theta)|_{\omega=0} = \mathcal{S}^*_{\mathcal{PP}} = [A, \ldots, A] \tag{21}$$

where $A = [a_1, \ldots, a_{N_g}]^\top$. To access the partition sub-matrices, one can write $[\mathcal{S}_{\mathcal{PP}}(\theta) \quad \epsilon\mathcal{S}_{\mathcal{PQ}}(\theta)] = W\mathcal{S}(\theta)M$ where $W = [I, \ 0]$ and $M = \text{blockdiag}([I, \ \epsilon I])$ and ϵ is a very small real number. It can be shown that:

$$\begin{aligned} \|W\mathcal{S}(\theta)M\|_\infty &= \|\mathcal{S}_{\mathcal{PP}}(\theta)\|_\infty + \epsilon^2 \|\mathcal{S}_{\mathcal{PQ}}(\theta)\|_\infty \\ &\approx \|\mathcal{S}_{\mathcal{PP}}(\theta)\|_\infty \end{aligned} \tag{22}$$

Consequently, the problem can be written as minimizing γ subject to:

$$\|W\mathcal{S}(\theta)M - [\mathcal{S}^*_{\mathcal{PP}}(\theta), \bar{0}]\|_\infty < \gamma \tag{23}$$

where $\bar{0}$ is a matrix with all elements set to zero. Similar to previous parts, this constraint can be written as:

$$\begin{bmatrix} \gamma & \Gamma_{k,i} \\ \Gamma^*_{k,i} & \Psi_{k,i} \end{bmatrix} \geq 0$$

$$\begin{aligned} \text{where } \Psi_{k,i} &= (M_k^{-1}Z_{k,i})^* M_k^{-1} Z_{ck,i} + \\ &\quad (M_k^{-1}Z_{ck,i})^* M_k^{-1} Z_{k,i} - (M_k^{-1}Z_{ck,i})^* M_k^{-1} Z_{ck,i} \\ \Gamma_{k,i} &= W_k Y_{k,i} - [\mathcal{S}^*_{\mathcal{PP}}, \ \bar{0}] M_k^{-1} Z_{k,i} \end{aligned} \tag{24}$$

for $k = \{1, 2, \ldots, N_\omega\}$ and $i = \{1, 2, \ldots, N_\theta\}$. However, as the power-sharing is usually considered as a steady-state feature, this constraint should be satisfied in low frequencies (e.g. it can only be satisfied for the first frequency point in the frequency grid).

The complete controller design problem can be written as

$$\begin{aligned} &\min \gamma \\ \text{subject to: } &\begin{bmatrix} \gamma & \Gamma_{1,i} \\ \Gamma^*_{1,i} & \Psi_{1,i} \end{bmatrix} \geq 0 \\ &\begin{bmatrix} I & W_{1k}Y_{k,i} \\ (W_{1k}Y_{k,i})^* & \bar{Z}_{k,i} \end{bmatrix} > 0 \\ &\begin{bmatrix} I & W_{2k}X_{k,i} \\ (W_{2k}X_{k,i})^* & \bar{Z}_{k,i} \end{bmatrix} > 0 \\ &\bar{Y}_{k,i} > 0, \end{aligned} \tag{25}$$

for $k = \{1, 2, \ldots, N_\omega\}$ and $i = \{1, 2, \ldots, N_\theta\}$. It should be noted that the last constraint is added for providing stability as explained in Section 2.

4. CASE STUDY

The performance of the proposed method is verified through simulation of an MG including an SG, a BESS and a PV unit shown in Fig. 1. The grid parameters are mentioned in Table. 1. It should be noted that the parameters mentioned here have just been used for simulation and not for the controller design. The data for design has been generated by non-linear numerical simulation of the MG using Simscape library of Matlab Simulink. The scheduling parameters could be potentially voltage magnitudes and phases. In order to reduce the complexity of the problem, the active power reference for the closed-loop system has been selected as the scheduling parameter. The process of data acquisition from the grid has been done through simulating the plant in different operating points while injecting a small excitation to the plant. For the excitation, a multi-period Pseudo-Random Binary Sequence (PRBS) signal is employed. The frequency response corresponding to each operating point is calculated using (1). In this case study, two DGs are controlled, which results in four inputs four outputs plant. As an example, the response of SG output power around the first working point, while applying excitation to its reference frequency, is shown in Fig. 2. The corresponding bode diagram is depicted in Fig. 3. The controller design parameters are mentioned in Table 2. In this case study, the total identification and solving the problem (25) takes less than 3 hours using a desktop computer. The performance of the proposed LPV Data-Driven (LPVDD) controller is compared with two other controllers: 1) droop controller, 2) a non-LPV Data-Driven (DD) controller that is designed with the same method but for a nominal working point. In Fig. 4, the SG frequency is shown at the time of load change. It can be seen that the LPV controller has less frequency nadir and oscillation compared with the other controllers. The

Table 1. Case study system parameters

BESS (Bus 4)	
Output filter:	$R_t = 10\text{m}\Omega$, $L_t = 450\ \mu\text{H}$
	$R_g = 58\text{m}\Omega$, $L_g = 420\ \mu\text{H}$, $C_f = 50\ \mu\text{F}$
Time Constants:	$\tau_\omega = 5 \cdot 10^{-4}$, $\tau_U = 5 \cdot 10^{-4}$
Nom. apparent power:	2.5 MVA
PV(Bus 1)	
Output filter:	$R_t = 10\text{m}\Omega$, $L_t = 450\ \mu\text{H}$
	$R_g = 58\text{m}\Omega$, $L_g = 420\ \mu\text{H}$, $C_f = 50\ \mu\text{F}$
Active Power:	10 kW
Load (Bus 2,3)	
Load powers:	[100δ,50δ] kW
scaling factor (δ)	$[1, \ldots, 9]$
Line Impedance[$m\Omega$]	
[1-2, 2-3, 3-4, 2-5]	[18+j3.4, 450+j85, 90+j17, 300+j220]
SG (Bus 5)	
Inertia Constant:	H = 1.5
Time Constants:	$\tau_m = 0.1$, $\tau_U = 0.05$
Speed Controller:	$k_p = 3.18$, $k_i = 4.77$, k_d=0.8, $T_f = 0.05$
Nom. apparent power:	2.5 MVA

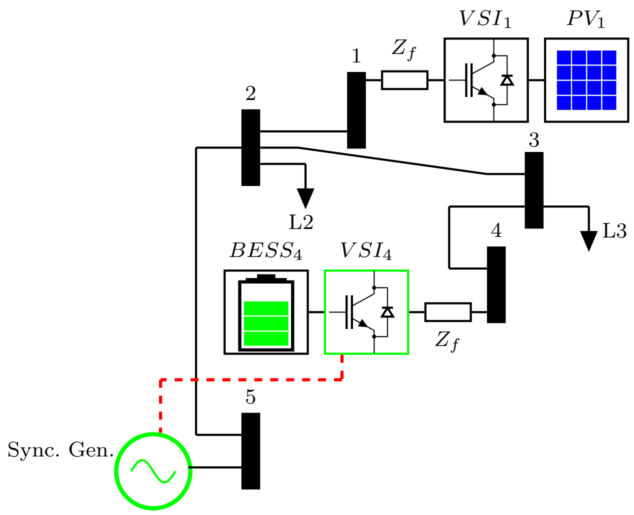

Fig. 1. Case study MG (solid line: power line, dashed line: communication, L_i: load, Z_f: LCL filter)

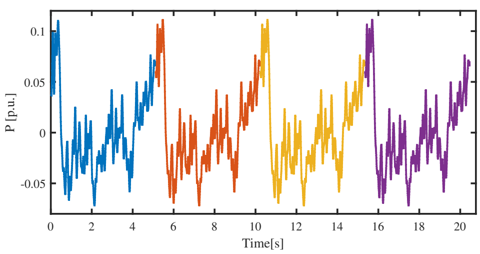

Fig. 2. Output power at bus No 5

power-sharing performance is compared in Fig. 5. As it can be seen, the LPV controller has less oscillation in general and less overshoot in the inverter.

5. CONCLUSIONS

In this paper, a data-driven method for multivariable LPV control synthesis in frequency-domain is proposed. This method was applied to the combined primary/secondary MG control design problem. Using this method, a controller is designed for a non-linear system with no need for a parametric model and only by using the input-output measurement data in different operating points. Using this method, the stability is guaranteed for frozen scheduling parameter while for the general case of time-varying scheduling parameter there is no guarantee for stability. However, it has been shown through simulation that based on the proposed choice of scheduling parameter, the controller can be applied to the MG control problem successfully. The case study includes an SG, BESS, PV

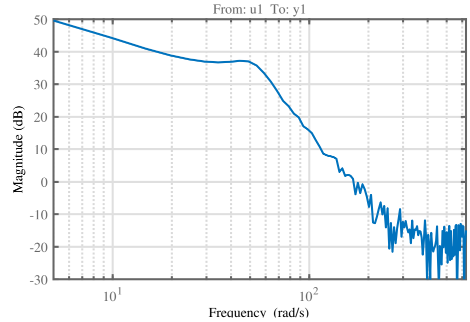

Fig. 3. Frequency response of output power of SG to frequency reference

Table 2. Identification and Design Parameters

PRBS [order, periods]	[10,4]
$[N_\theta, N_\omega, n_\rho, \delta, \epsilon, T_s]$	[9, 291, 1, 20,0.1, 5 ms]
W_1	-5dB I for all frequencies
W_2	diag([80 dB,80 dB,35 dB, 35 dB])
	for $\omega < 2$ rad/sec
	35dB I for $\omega \geq 2$ rad/sec
X_c	$\text{diag}([10^{-3}, 10^{-3}, 2\times 10^{-3}, 2\times 10^{-3}])z^{20}$
$[Y_c, F_x, F_y]$	$[Iz^{20},\ \bar{1},\ \bar{1}]$

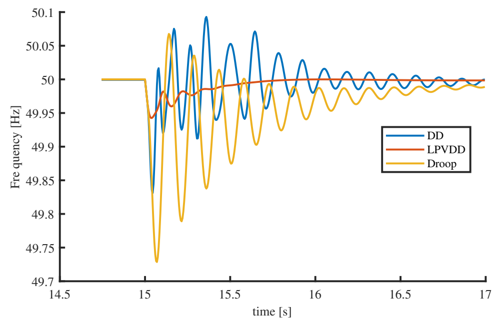

Fig. 4. Frequency of SG when load changes

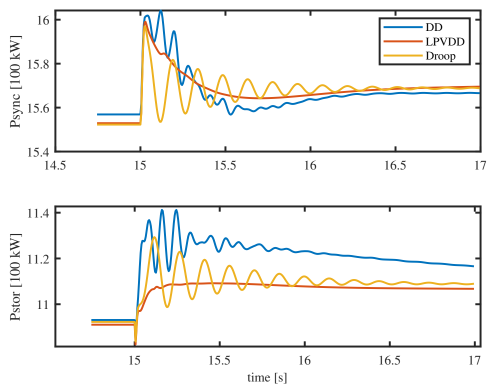

Fig. 5. Power-sharing between SG and BESS

unit and different loads. The results show that this controller has good performance in a wide range of operating points.

REFERENCES

Ainsworth, N. and Grijalva, S. (2013). A structure-preserving model and sufficient condition for frequency synchronization of lossless droop inverter-based ac networks. *IEEE Trans. Power Syst.*, 28(4), 4310–4319.

Apkarian, P. and Noll, D. (2018). Structured H_∞-control of infinite-dimensional systems. *Int. J. Robust Nonlin.*, 28(9), 3212–3238. doi:10.1002/rnc.4073.

Berberich, J., Romer, A., Scherer, C.W., and Allgöwer, F. (2019). Robust data-driven state-feedback design. 1–7. URL http://arxiv.org/abs/1909.04314.

Butcher, M. and Karimi, A. (2009). Data-driven tuning of linear parameter varying precompensators. *Int. J. Adapt. Contr. Signal Process.*, 24.

Campi, M., Lecchini, A., and Savaresi, S. (2002). Virtual reference feedback tuning: a direct method for the design of feedback controllers. *Automatica*, 38(8), 1337 – 1346.

Chandorkar, M.C., Divan, D.M., and Adapa, R. (1993). Control of parallel connected inverters in standalone ac supply systems. *IEEE Trans. Ind. Appl.*, 29(1), 136–143.

Chang, C.Y. and Zhang, W. (2016). Distributed control of inverter-based lossy microgrids for power sharing and frequency regulation under voltage constraints. *Automatica*, 66, 85–95.

Coulson, J., Lygeros, J., and Dörfler, F. (2018). Data-Enabled Predictive Control: In the Shallows of the DeePC. URL http://arxiv.org/abs/1811.05890.

Dai, T. and Sznaier, M. (2019). A Moments Based Approach to Designing MIMO Data Driven Controllers for Switched Systems. In *Proceedings of the IEEE Conference on Decision and Control*, volume 2018-December, 5652–5657. Institute of Electrical and Electronics Engineers Inc. doi:10.1109/CDC.2018.8619361.

Formentin, S., Heusden, K., and Karimi, A. (2014). A comparison of model-based and data-driven controller tuning. *Int. J. Adapt. Contr. Signal Process.*, 28.

Formentin, S., Piga, D., Tóth, R., and Savaresi, S.M. (2016). Direct learning of LPV controllers from data. *Automatica*, 65, 98 – 110.

Formentin, S. and Savaresi, S.M. (2011). Virtual reference feedback tuning for linear parameter-varying systems. *IFAC Proceedings Volumes*, 44(1), 10219 – 10224. 18th IFAC World Congress.

Goncalves Da Silva, G.R., Bazanella, A.S., Lorenzini, C., and Campestrini, L. (2019). Data-Driven LQR Control Design. *IEEE Control Systems Letters*, 3(1), 180–185. doi:10.1109/LCSYS.2018.2868183.

Guo, X., Lu, Z., Wang, B., Sun, X., Wang, L., and Guerrero, J.M. (2014). Dynamic phasors-based modeling and stability analysis of droop-controlled inverters for microgrid applications. *IEEE Trans. Smart Grid*, 5(6), 2980–2987.

Hjalmarsson, H., Gunnarsson, S., and Gevers, M. (1994). A convergent iterative restricted complexity control design scheme. In *Proceedings of 1994 33rd IEEE Conference on Decision and Control*, volume 2, 1735–1740 vol.2.

Hoffmann, C. and Werner, H. (2015). A survey of linear parameter-varying control applications validated by experiments or high-fidelity simulations. *IEEE Trans. Control Syst. Technol.*, 23(2), 416–433.

Karimi, A. and Emedi, Z. (2013). h_∞ gain-scheduled controller design for rejection of time-varying narrow-band disturbances applied to a benchmark problem. *Eur. J. Control*, 19, 279–288.

Karimi, A. and Galdos, G. (2010). Fixed-order H_∞ controller design for nonparametric models by convex optimization. *Automatica*, 46(8), 1388 – 1394.

Karimi, A. and Kammer, C. (2017). A data-driven approach to robust control of multivariable systems by convex optimization. *Automatica*, 85, 227–233.

Katiraei, F. and Iravani, M.R. (2006). Power management strategies for a microgrid with multiple distributed generation units. *IEEE Trans. Power Syst.*, 21(4), 1821–1831.

Keel, L.H. and Bhattacharyya, S.P. (2008). Controller synthesis free of analytical models: Three term controllers. *IEEE Trans. Autom. Control*, 53(6), 1353–1369.

Kergus, P., Olivi, M., Poussot-Vassal, C., and Demourant, F. (2019). From reference model selection to controller validation: Application to Loewner data-driven control. *IEEE Contr. Syst. Lett.*, 3(4), 1008–1013.

Olivares, D.E., Mehrizi-Sani, A., Etemadi, A.H., Cañizares, C.A., Iravani, R., Kazerani, M., Hajimiragha, A.H., Gomis-Bellmunt, O., Saeedifard, M., Palma-Behnke, R., et al. (2014). Trends in microgrid control. *IEEE Trans. on smart grid*, 5(4), 1905–1919.

Pang, B., Bian, T., and Jiang, Z.P. (2019). Data-driven Finite-horizon Optimal Control for Linear Time-varying Discrete-time Systems. In *Proceedings of the IEEE Conference on Decision and Control*, volume 2018-December, 861–866. Institute of Electrical and Electronics Engineers Inc. doi:10.1109/CDC.2018.8619347.

Safonov, M.G. and Tsao, T.C. (1997). The unfalsified control concept and learning. *IEEE Trans. Autom. Control*, 42(6), 843–847. doi:10.1109/9.587340.

Salvador, J.R., de la Peña, D.M., Alamo, T., and Bemporad, A. (2018). Data-based predictive control via direct weight optimization∗. *IFAC-PapersOnLine*, 51(20), 356–361. doi:10.1016/j.ifacol.2018.11.059.

Schiffer, J., Ortega, R., Astolfi, A., Raisch, J., and Sezi, T. (2014). Conditions for stability of droop-controlled inverter-based microgrids. *Automatica*, 50(10), 2457–2469.

Shamma, J.S. and Athans, M. (1992). Gain scheduling: potential hazards and possible remedies. *IEEE Control Syst. Mag.*, 12(3), 101–107. doi:10.1109/37.165527.

Simpson-Porco, J.W., Dörfler, F., and Bullo, F. (2013). Synchronization and power sharing for droop-controlled inverters in islanded microgrids. *Automatica*, 49(9), 2603–2611.

van Heusden, K., Karimi, A., and Bonvin, D. (2011). Data-driven model reference control with asymptotically guaranteed stability. *Int. J. Adapt. Contr. Signal Process.*, 25(4), 331–351.

van Solingen, E., van Wingerden, J., and Oomen, T. (2018). Frequency-domain optimization of fixed-structure controllers. *Int. J. Robust Nonlin.*, 28(12), 3784–3805.

Xie, W. and Eisaka, T. (2004). Design of lpv control systems based on youla parameterisation. *IET Control Theory A.*, 151(4), 465–472.

APPENDIX C

Data-Driven Distributed Reactive Power Sharing in Microgrids

Published in the Proceedings of IEEE Conference on Decision and Control (2019)

Data-Driven Distributed Reactive Power Sharing in Microgrids

Seyed Sohail Madani and Alireza Karimi

Abstract— **In this paper, reactive power sharing for Photovoltaic (PV) units in islanded microgrids has been formulated as a robust control design problem and is solved using convex optimization method. In addition to reactive power sharing, the disturbance rejection for voltage and active power have been formulated using infinity-norm constraints on the sensitivity functions and considered in the design. The proposed method uses only the measurement data of the power system with no need for a parametric model of the power grid equipment. The size of the problem is independent of the order of the plant which makes it applicable to power systems including a high number of buses and equipment such as synchronous generators, batteries and inverters. In the proposed method, the communication system can be considered in the control design process for centralized, distributed and decentralized structures. The proposed method has been validated through simulation of a microgrid encompassing synchronous generator, switching inverters and storage system. The results show that this method has successfully shared reactive power among different PV units while providing disturbance rejection for voltage and active power.**

I. INTRODUCTION

Global warming concerns has led to increase the share of renewable energy resources in electrcity generation. Except for hydro energy plants, most of renewable Distributed Generation units (DGs) such as PVs and the wind turbines are connected to the power grid using power-electronic converters. Since the renewable resources are intermittent, the ratings for different parts of the system are designed for maximum power, while the system usually does not operate in its full capacity. The priority for using the capacity of the equipment is with active power. However, the spare capacity of the converters can be used to provide ancillary services to the grid including reactive power compensation.

Traditionally, the reactive power in the distribution grid is provided by constant or switchable capacitor banks. Since the constant capacitors inject almost a constant reactive power, they may cause overvoltage when the system is not fully loaded. In switchable capacitor banks, the number of the possible steps are limited and causes high inrush current, over-voltages and harmonics [1]. As another solution, Static Var Compensators (SVCs) have been proposed to compensate the reactive power in distribution systems [2]–[4]. However, high harmonic injection and very low bandwidth are reported in industrial types of SVCs [3]. Distribution STATic synchronous COMpensator (D-STATCOM) [5], [6] improves the power quality and supports reactive power with high bandwidth. However, due to high investment costs, the applications are limited and the size of this equipment should be selected conservatively [7].

Instead of adding equipment, the spare capacity of power electronic converters of DGs can be used to compensate for reactive power [8]. However, sharing the reactive power among different DGs with the aim of avoiding converter overload is a challenging control problem. Different methods have been proposed for control of reactive power and sharing this power among DGs. A group of proposed methods are based on the idea of droop control [9], [10]. Although these methods are simple and easy to implement, the closed-loop stability is not generally guaranteed. A sliding mode controller has been proposed in [11] for reactive power control of wind turbines. In [12], high-level optimal reactive power control has been proposed assuming each DGs can regulate the injected power to the grid. In [13], the stability boundaries of a wind power plant including a STATCOM and controlled by PI controller as voltage controllers have been assessed with the aim to damp the low-frequency reactive power oscillations. An adaptive control method for a wind turbine has been proposed in [14] for reactive power compensation while guaranteeing performance and boundedness of the signals. However, these methods need parametric models which are usually hard to achieve in power systems. In [15], a non-linear state feedback controller using communication system has been proposed in order to share the reactive power among different inverters in a distributed way. In [16], the reactive power has been controlled in order to be in maximum distance from the voltage bifurcation point to avoid the voltage collapse. However, the couplings in the power-flow equation have not been considered, which can be significant in distribution systems.

In this paper, a data-driven controller design method for the reactive power sharing problem is proposed. The reactive power sharing and other control performance are formulated using the infinity-norm bounds on input and output sensitivity functions. Then, the problem is written in the concave-convex form and the concave part is linearized around an initial controller. Finally, the control problem is converted to a convex optimization problem with linear matrix inequalities (LMIs). In this method, there is no need for a parametric model of the power system and only measurement data is used in the design process. Moreover, there is no need for any assumption on the decoupling of active power from voltage and reactive power from frequency in this method, which makes it applicable to different distribution as well

This work is supported in part by the Swiss National Science Foundation under Grant 200021_172828 and by Swiss Federal Commission for Innovation and Technology within the SCCER-FURIES. *(Corresponding author: Alireza Karimi.)*

S. S. Madani and A. Karimi are with the Laboratoire d' Automatique, École Polytechnique Fédérale de Lausanne, 1015 Lausanne, Switzerland (e-mail: sohail.madani@epfl.ch; alireza.karimi@epfl.ch).

as transmission systems. Another significant advantage of this method is the capability of designing the controller for centralized, distributed or decentralized structures based on the availability of communication infrastructure.

The rest of the paper is organised as follows: In Section II, the data-driven controller design method has been described. In Section III, the reactive power sharing problem for PV units in power grids has been formulated as a set of LMIs. In Section IV, a controller has been designed for the case-study grid and its performance has been validated in simulation. Finally, the conclusions are presented in SectionV.

II. Controller Design

The design method in this paper is based on the frequency response of the system. If the parametric model is available the frequency response can be directly calculated. Since the parameters of the power system are not usually easy to extract, the frequency response is computed using the measurement data. Because the measurement data in a short time usually is not rich enough, adding an excitation signal can increase the accuracy of the frequency response. In this paper, a Pseudo-Random Binary Sequence (PRBS) has been used as the external excitation. Using the Fourier transform, an m-input/n-output frequency response model $G(e^{j\omega}) \in \mathbb{C}^{n\times m}$ around the operating point is calculated.

A. Controller Structure

The general structure of the controller is $K = XY^{-1}$ where X and Y are matrix polynomials in z (or in s for continuous-time controllers). For sake of simplicity in notation, the argument of $e^{j\omega}$, z or s are omitted and will only be reiterated when it deemed necessary. This controller can be designed in centralized, distributed or decentralized structures based on the available communication links. If the communication link is not available between two points the corresponding element in the controller is fixed to zero.

B. Sensitivity Functions

The control design problem formulation in this paper is based on the method proposed in [17]. The goal is to formulate the control design problem in the form of a convex optimization problem. Considering the filtered output sensitivity, the controller design problem can be written as:

$$\min_{K} \|W_L S W_R\|_\infty \tag{1}$$

where $S = (I+GK)^{-1}$ is the output sensitivity function, W_L and W_R are the left and right weighting filters, where W_R is assumed to be invertible. The infinity-norm constraint can be converted to a spectral norm and be approximated with a finite number N of frequencies in Ω_N such that:

$$\Omega_N \subset \Omega = \left\{\omega \,\middle|\, -\frac{2\pi}{T_s} < \omega < \frac{2\pi}{T_s}\right\} \setminus B_g \setminus B_y$$

where B_g and B_y are respectively the set of finite frequencies in which G and Y are unbounded. It can be shown that the problem in (1) can be written as:

$$\begin{aligned} &\min_{X,Y,\gamma} \gamma \\ &\text{s.t. } (W_{Lk}S_k W_{Rk})^* (W_{Lk}S_k W_{Rk}) \le \gamma I \end{aligned} \tag{2}$$

for $k = 1, \dots, N$, where $S_k := S(e^{j\omega})|_{\omega=\omega_k}$. The other variables with subscript k are defined similarly. Replacing K with XY^{-1} and defining $E = Y - GX$, (2), one obtains:

$$(W_{Lk}Y_k)^*\gamma^{-1}W_{Lk}Y_k - (W_{R_k}^{-1}E_k)^* W_{R_k}^{-1}E_k \le 0 \tag{3}$$

Using Schur complement lemma, (3) can be written as:

$$\begin{bmatrix} \gamma I & W_{Lk}Y_k \\ (W_{Lk}Y_k)^* & (W_{R_k}^{-1}E_k)^*(W_{R_k}^{-1}E_k) \end{bmatrix} \ge 0 \tag{4}$$

The quadratic term can be linearized around an initial stabilizing controller $K_c = X_c Y_c^{-1}$ [17] as follows:

$$(W_{R_k}^{-1}E_k)^*(W_{R_k}^{-1}E_k) \ge F_k \tag{5}$$

where

$$\begin{aligned} F_k = &(W_{R_k}^{-1}E_k)^* W_{R_k}^{-1}E_{ck} + (W_{R_k}^{-1}E_{ck})^*(W_{R_k}^{-1}E_k) \\ &- (W_{R_k}^{-1}E_{ck})^*(W_{R_k}^{-1}E_{ck}) \end{aligned}$$

and $E_c = Y_c + GX_c$. Then, the problem (1) can be represented by the following convex optimization problem:

$$\begin{aligned} &\min_{X,Y,\gamma} \gamma \\ &\text{s.t. } \begin{bmatrix} \gamma I & W_{Lk}Y_k \\ (W_{Lk}Y_k)^* & F_k \end{bmatrix} \ge 0 \text{ , for } k = 1, \dots, N \end{aligned} \tag{6}$$

For limiting the impact of disturbances on control signals, the input sensitivity function can be limited by defining a constraint on $U = K(I + GK)^{-1}$ as:

$$\|W_U U\|_\infty < 1 \tag{7}$$

where W_U is the weighting filter corresponding the input sensitivity function. Similar to the previous part, this constraint can be written as:

$$\begin{bmatrix} I & W_{Uk}X_k \\ (W_{Uk}X_k)^* & E_k^* E_{ck} + E_{ck}^* E_k - E_{ck}^* E_{ck} \end{bmatrix} \ge 0, \tag{8}$$

for $k = 1, \dots, N$.

C. Stability

In [17], it has been proved that the closed-loop system with the controller $K = XY^{-1}$ and the plant model G is stable if:

1) the initial controller $K_c = X_c Y_c^{-1}$ is stabilizing,
2) $E^* E_c + E_c^* E > 0, \forall\omega \in \Omega$
3) $\det(Y_c) \neq 0$ and $\det(Y) \neq 0$ $\forall\omega \in \Omega$
4) $\det(Y) = \det(Y_c) = 0$ $\forall\omega \in B_y$
5) the order of $\det(Y_c) =$ the order of $\det(Y)$

It should be mentioned that Condition 2 is always satisfied because it appears in the infinity-norm constraints. However, Condition 3 should be met by imposing $Y^*Y > 0$. This can be achieved using the following LMI:

$$Y^*Y_c + Y_c^*Y - Y_c^*Y_c > 0, \qquad \forall\omega \in \Omega \tag{9}$$

III. Reactive Power Sharing Problem

The objective of the control system of a microgrid is to supply power to loads while keeping voltage magnitude within standard bounds and voltage angle bounded in order to keep synchronism. A general structure of the control system for a microgrid is shown in Fig. 1. This structure is related to an islanded microgrid including synchronous generator, battery storage and PV units. In this structure, G^v_{PV}, G^v_{B} and G^v_{S} are the transfer functions from voltage reference of PV inverter, battery inverter and synchronous generator (i.e. $\bar{v}_{\mathrm{PV}}$, $\bar{v}_{\mathrm{B}}$, and $\bar{v}_{\mathrm{S}}$) to the corresponding output voltages (i.e. v_{PV}, v_{B}, and v_{S}). Similarly, G^θ_{PV}, G^θ_{B} and G^θ_{S} are the transfer functions from voltage angle references of PV inverter, battery inverter and synchronous generator (i.e. $\bar{\theta}_{\mathrm{PV}}$, $\bar{\theta}_{\mathrm{B}}$, and $\bar{\theta}_{\mathrm{S}}$) to the corresponding voltage angles (integral of electrical frequency) (i.e. θ_{PV}, θ_{B}, and θ_{S}). G_g is the transfer function from nodal voltage magnitude and angle at different buses to the active and reactive power injected into the grid. The parametric models related to these transfer functions are developed in [18]. K_d is the droop controller for synchronous generator and battery and K_S represents the synchronous generator internal speed controller. G_{LD} is the disturbance transfer function from the load powers (i.e. $[P_L, P_Q]^T$) to the output powers of G_g. The active and reactive power references for battery and synchronous generator (i.e. $[\bar{P}_B, \bar{P}_S, \bar{Q}_B, \bar{Q}_B]$) are usually generated by higher level optimization algorithms (e.g. Optimal Power Flow (OPF)), which is not in the scope of this paper. The references of active power for PV buses (i.e. $\bar{P}_{\mathrm{PV}}$) are related to solar irradiation and the level of the dc-link voltage, which have high fluctuations. The reactive power references of the PV units (i.e. $\bar{Q}_{\mathrm{PV}}$) may be selected based on the outcome of OPF, which are usually updated every few minutes. Controller K is responsible for setting the electrical angles and voltage magnitudes so that the reactive power of the loads are shared proportionally among different PV units.

A. Reactive Power Sharing Formulation

When the reactive power consumption/injection of the loads are changed, it should be shared among different PV units. Based on the structure mentioned in the previous section for a power grid with n_{PV}-PV units one can write:

$$\left[\bar{v}_{\mathrm{PV}},\ \bar{\theta}_{\mathrm{PV}}\right]^T = K\left[P_{\mathrm{e}},\ Q_{\mathrm{e}}\right]^T \tag{10}$$

where $[P_{\mathrm{e}},\ Q_{\mathrm{e}}]^T = \left[\bar{P}_{\mathrm{PV}},\ \bar{Q}_{\mathrm{PV}}\right]^T - [P_{\mathrm{PV}},\ Q_{\mathrm{PV}}]^T$ and each variable is a $n_{\mathrm{PV}} \times 1$ vector. (e.g. $\bar{P}_{\mathrm{PV}} = \left[\bar{P}^1_{\mathrm{PV}}, \cdots, \bar{P}^{n_{\mathrm{PV}}}_{\mathrm{PV}}\right]^T$ and the other variables are defined similarly). The input and output of U are given as:

$$\left[\bar{v}_{\mathrm{d}},\ \bar{\theta}_{\mathrm{PV}}\right]^T = U\left[P_{\mathrm{d}},\ Q_{\mathrm{d}}\right]^T \tag{11}$$

where $[P_{\mathrm{d}},\ Q_{\mathrm{d}}]^T = \left[P^1_{\mathrm{d}}, \cdots, P^{n_{\mathrm{PV}}}_{\mathrm{d}}, Q^1_{\mathrm{d}}, \cdots, Q^{n_{\mathrm{PV}}}_{\mathrm{d}}\right]^T$. Similarly, for the output sensitivity function one can write:

$$\left[P_{\mathrm{e}},\ Q_{\mathrm{e}}\right]^T = S\left[P_{\mathrm{d}},\ Q_{\mathrm{d}}\right]^T \tag{12}$$

In order to share the reactive power disturbance among different PV units, each unit should have an error with

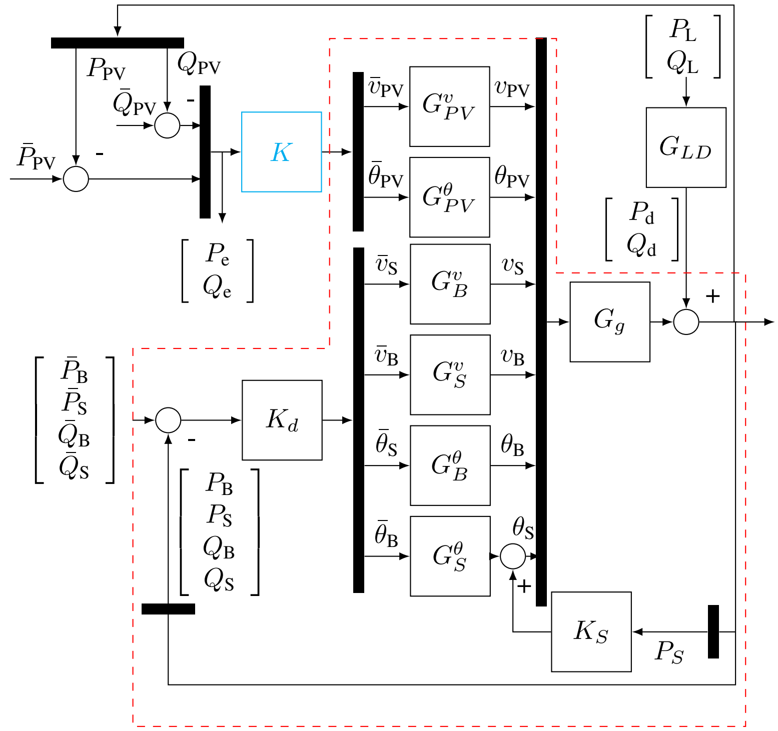

Fig. 1. General structure of the microgrid control system

respect to its reference to compensate the reactive power mismatch until the next output command of OPF. In order to have the impact of reactive power disturbance on reactive power error, one can write

$$[0_{n_{\mathrm{PV}}}, Q_{\mathrm{e}}]^T = W^Q_L S W^Q_R\left[P_{\mathrm{d}},\ Q_{\mathrm{d}}\right]^T \tag{13}$$

where $W^Q_L = \mathrm{diag}\{0_{n_{\mathrm{PV}}}, I_{n_{\mathrm{PV}}}\}$ and $W^Q_R = \mathrm{diag}\{0_{n_{\mathrm{PV}}}, I_{n_{\mathrm{PV}}}\}$. The sharing can be based on any arbitrary preference of the controller designer. We assume that the PV units connected to one microgrid are close to each other and have almost the same per unit spare capacity. Consequently, sharing the reactive power proportional to nominal power can be a reasonable choice. It can be shown that if the following condition holds, the steady-state nominal reactive power sharing can be achieved:

$$W^Q_L S W^Q_R\Big|_{\omega=0} = S_{\mathrm{RPS}} \tag{14}$$

$$\text{where}\qquad S_{\mathrm{RPS}} = \begin{bmatrix} 0_{n_{\mathrm{PV}}} & 0_{n_{\mathrm{PV}}} \\ 0_{n_{\mathrm{PV}}} & \begin{matrix} \frac{\mathrm{VA}^1_{\mathrm{nom}}}{\mathrm{VA}^{\mathrm{tot}}_{\mathrm{nom}}} & \cdots & \frac{\mathrm{VA}^1_{\mathrm{nom}}}{\mathrm{VA}^{\mathrm{tot}}_{\mathrm{nom}}} \\ \vdots & \vdots & \vdots \\ \frac{\mathrm{VA}^{n_{\mathrm{PV}}}_{\mathrm{nom}}}{\mathrm{VA}^{\mathrm{tot}}_{\mathrm{nom}}} & \cdots & \frac{\mathrm{VA}^{n_{\mathrm{PV}}}_{\mathrm{nom}}}{\mathrm{VA}^{\mathrm{tot}}_{\mathrm{nom}}} \end{matrix} \end{bmatrix}$$

and VA^1 is the nominal apparent power of i-th PV unit and $\mathrm{VA}^{\mathrm{tot}}_{\mathrm{nom}} = \sum_{i=1}^{i=n_{\mathrm{PV}}} \mathrm{VA}^i$.

B. Controller Design Problem for Reactive Power Sharing

Based on the method described in Section II the controller design problem can be defined as:

$$\min_K \left| W^Q_L S(e^{j\omega_1}) W^Q_R - S_{\mathrm{RPS}} \right| \tag{15}$$

where $\omega_1 = 0$. In order to add tracking and disturbance rejection to the controller, the problem can be written as:

$$\|W_S S\|_\infty < 1 \tag{16}$$

For limiting the impact of disturbance on voltage and angle, the following constraint can be added:

$$\|W_U U\|_\infty < 1 \tag{17}$$

Using (6) and (8) and considering (16-12), the problem can be written as:

$$\min_{X,Y,\gamma} \gamma \tag{18}$$

$$\text{s.t.} \begin{bmatrix} \gamma I & W_L^Q Y_1 \\ (W_L^Q Y_1)^* & F_1 \end{bmatrix} \geq 0$$
$$\begin{bmatrix} I & W_{Sk} Y_k \\ (W_{Sk} Y_k)^* & E_k^* E_{ck} + E_{ck}^* E_k - E_{ck}^* E_{ck} \end{bmatrix} \geq 0$$
$$\begin{bmatrix} I & W_{Uk} X_k \\ (W_{Uk} X_k)^* & E_k^* E_{ck} + E_{ck}^* E_k - E_{ck}^* E_{ck} \end{bmatrix} \geq 0$$
$$Y_k^* Y_{c,k} + Y_{c,k}^* Y_k - Y_{c,k}^* Y_{c,k} > 0, \quad \forall \{k | \omega_k \in \Omega_N\}$$

where

$$\begin{aligned} F_1 =& ((W_R^Q)^{-1} E_1)^* (W_R^Q)^{-1} E_{ck} \\ &+ ((W_R^Q)^{-1} E_{c1})^* ((W_R^Q)^{-1} E_1) \\ &- ((W_R^Q)^{-1} E_{c1})^* ((W_R^Q)^{-1} E_{c1}) \end{aligned}$$

and $W_L^Q = \text{diag}\{0_{n_{\text{PV}}}, I_{n_{\text{PV}}}\}$ and $W_R^Q = \text{diag}\{\beta I_{n_{\text{PV}}}, I_{n_{\text{PV}}}\}$. β is relatively small scaler used to make W_R^Q invertible.

IV. Case Study

In order to validate the performance of the proposed method, it is applied on a case study microgrid through simulation via SimPower of Matlab Simulink. The inverters are modelled using switching elements driven by PWM. The single line diagram of the case study microgrid is shown in Fig. 2. This power distribution grid is composed of a synchronous generator, a battery energy storage unit and three PV units connected to different buses of the grid. The parameters of the grid are mentioned in Table I.

The X/R-ratio of different feeders in the grid are different and there is no assumption of dominantly resistive or inductive lines. In this case study, first the frequency response of the system is extracted from the measurements without using the parameters of the grid. Afterwards, the controller is designed and finally, the results are shown.

A. Measurements

An external excitation can be added to the inputs of the plant in order to find the frequency response of the system. In this case study, a multi-period PRBS signal with an amplitude of 0.01p.u. has been added to $\bar{v}_{\text{PV}}^1$, $\bar{v}_{\text{PV}}^2$, and $\bar{v}_{\text{PV}}^3$ and a PRBS signal with amplitude of 0.002 p.u. to $\bar{\theta}_{\text{PV}}^1$, $\bar{\theta}_{\text{PV}}^2$, and $\bar{\theta}_{\text{PV}}^3$ during 6 separate experiments. During each experiment, $[P_{\text{PV}},\ Q_{\text{PV}}]^T$ in p.u. are sampled with a frequency of 100 Hz. Taking the Fourier transform of the measured data, $G(j\omega) \in \mathbb{C}^{6\times 6}$ is calculated. In this case study, the frequency points are linearly distributed between 0 and 50 Hz. The order of PRBS signal is 7 (which is equivalent to 127 sample per period) and 5 periods has been applied. Consequently, the total duration of measurement is 38.1s ($= 127$(samples per periods) $\times$ 5(periods) $\times$ 10^{-2}(sampling time)$\times$6(inputs)). As an example, measured data corresponding to Q_{PV}^3 while adding last four periods of PRBS signal to $\bar{\theta}_{\text{PV}}^1$ and the resulting frequency response are shown in Fig. 3. The frequency response used for the controller design is the average of frequency responses of different periods at each frequency points.

TABLE I

CASE STUDY GRID PARAMETERS

Feeders	
Line between bus #1 and bus #2	$R = 0.3\Omega,\ X = 0.22\Omega$
Line between bus #2 and bus #3	$R = 0.018\Omega,\ X = 0.0034\Omega$
Line between bus #3 and bus #4	$R = 0.018\Omega,\ X = 0.0034\Omega$
Line between bus #4 and bus #5	$R = 0.15\Omega,\ X = 0.11\Omega$
Line between bus #6 and bus #7	$R = 0.09\Omega,\ X = 0.017\Omega$
Line between bus #7 and bus #8	$R = 0.09\Omega,\ X = 0.017\Omega$
Line between bus #1 and bus #6	$R = 0.3\Omega,\ X = 0.22\Omega$
Line between bus #2 and bus #7	$R = 0.45\Omega,\ X = 0.085\Omega$
BESS	
Bus #:	8
Output filter Parameters:	R_t = 10mΩ, L_t = 450 μH R_g = 58mΩ, L_g = 420 μH, C_f = 50 μF
Time Constants:	$\tau_\omega = 5 \cdot 10^{-4}$, $\tau_U = 5 \cdot 10^{-4}$
Nom. apparent power:	30 KVA
Synchronous Generator	
Bus #:	1
Inertia Constant:	H = 1.5
Internal Impedance:	R_o = 19mΩ, L_o = 2.7 mH
Time Constants:	$\tau_m = 0.1$, $\tau_U = 0.05$
Speed Controller:	k_p = 3.18, k_i = 4.77, k_d=0.8, T_f = 0.05
Nom. apparent power:	45 KVA
Inverter	
Bus #:	3,4,5,8
Switching Frequency:	15 KHz
DC Voltage:	325 V
PV	
Bus #:	3,4,5
Output filter Parameters:	R_t = 10mΩ, L_t = 450 μH R_g = 58mΩ, L_g = 420 μH, C_f = 50 μF
Nominal Power:	[30, 20, 40] kW
Loads	
Bus #:	3,6,7
Active/Reactive Power:	[30, 20, 25] kW / [0, 0, 0] VAr

B. Controller Design

The convex optimization problem in (18) has been solved based on the frequency response of the system using the measured data. An 8th order stabilizing initial controller with a very small gain is chosen:

$$Y_c = z^8 I_6,\ X_c = \epsilon z^8 I_6, K_c = X_c Y_c^{-1}$$

where $\epsilon = 0.05$. It should be noted that z^8 term in both Y_c and X_c has been added to satisfy the fourth stability condition.

The inverse of the weighing filter for output sensitivity function $W_{S_k}^{-1}$ for $\omega_k \in \Omega_N$ is selected as diag$(5\text{dB}I_3, I_3)$ for $\omega_k < BW$ where $BW = 15$ rad/s is the desired closed-loop bandwidth. For high frequencies, $\omega_k > BW$, the inverse of the weighting filter is chosen as $6\text{dB}I_6$ to limit

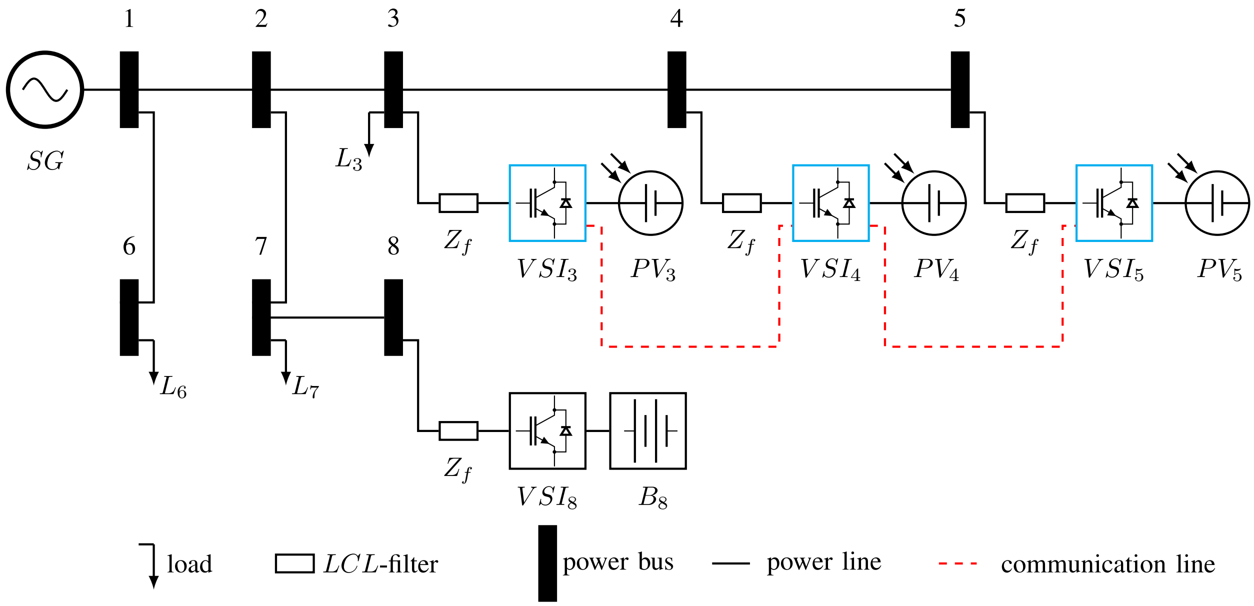

Fig. 2. Single line diagram of case study micro grid

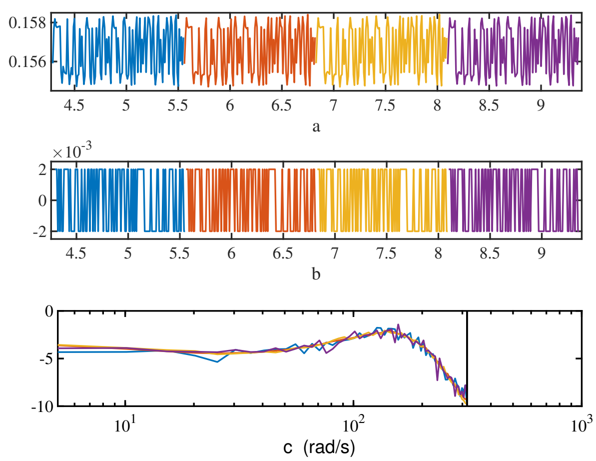

Fig. 3. a) measured data corresponding to Q^3_{PV}, b) last four periods of PRBS signal to $\bar{\theta}^1_{\mathrm{PV}}$ c) the corresponding frequency response

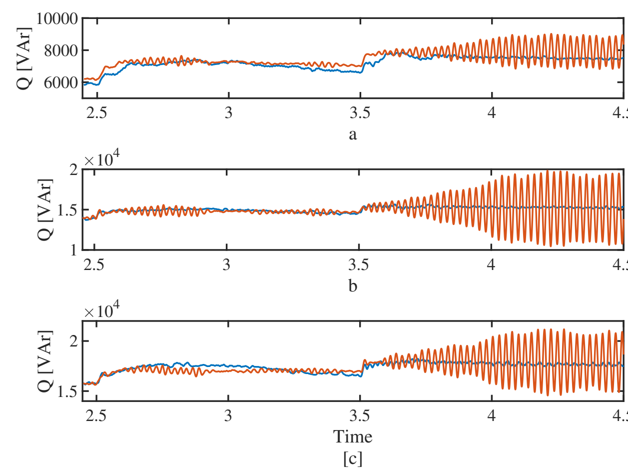

Fig. 4. Reactive power of three PV units, blue: proposed method, red: primary droop and secondary central integrator, a) reactive power of PV number 1, b) reactive power of PV number 2, c) reactive power of PV number 3

the maximum singular value of S to 6dB and obtaining a good stability margin. In order to limit the impact of high frequency harmonics on voltages and angles, the inverse of the weighting filter for input sensitivity function ${W_U}_k^{-1}$ is selected as 20dBI_6 for $\omega_k < 7 \times BW$ and I_6 for $\omega_k > 7 \times BW$.

C. Distributed Structure

As shown in Fig. 2, the system in the case study has distributed control structure. In this system, the data can be transferred between controllers of bus number 3 and bus number 4 as well as between 4 and 5 but there exists no data link between the inverters at bus number 3 and bus number 5. This structure is considered in the controller design process by setting the corresponding parameters to zero where there is no communication link.

D. Results

The performance of the designed controller has been validated through simulation using Matlab Simulink and are compared with conventional droop control as primary control combined with a central integrator as the secondary controller. To test the reactive power sharing performance, a 0.1 p.u. reactive load has been added to bus number 6 at t=2.5s and another 0.1 p.u. reactive load has been added to bus number 3 at t=3.5s. The reactive powers of the three PV units are shown in Fig. 4. It can be seen that the reactive powers have been shared based on their nominal apparent

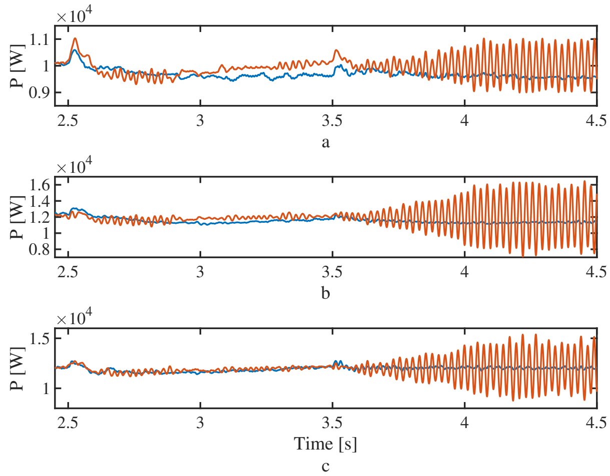

Fig. 5. Active power of three PV units. blue: proposed method, red: primary droop and secondary central integrator, a) active power of PV number 1, b) active power of PV number 2, c) active power of PV number 3

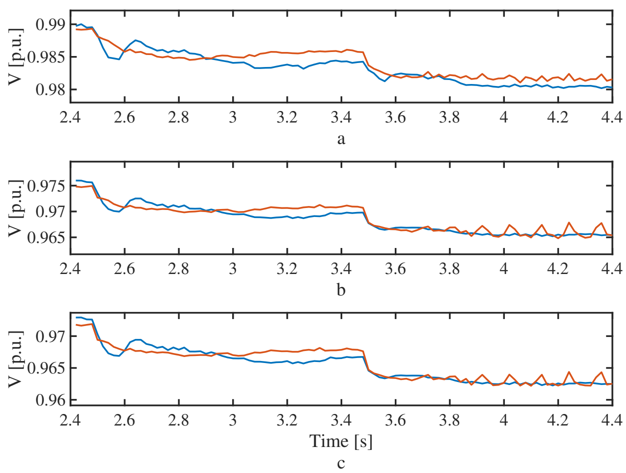

Fig. 6. RMS p.u. voltage of three PV units, blue: proposed method, red: primary droop and secondary central integrator, a) voltage of PV number 1, b) voltage of PV number 2, c) voltage of PV number 3

powers. As mentioned earlier, the droop control does not guarantee stability and it can be seen in this case study that the droop control fails to control reactive power after adding the second load to the system. The active powers of three PV after load disturbance are shown in Fig. 5. As shown in the figure, the controller rejects the disturbance on active power which leads to less stress of DC-link while the droop controller has a higher peak in active power and oscillatory mode after adding the second load. The RMS voltages of PV buses are shown in Fig. 6. As shown in this figure, voltages of PV units are kept within the standard band while the droop controller shows high fluctuations in voltage.

V. Conclusions

In this paper, a data-driven controller design approach has been proposed in order to employ the spare capacity of PV units in reactive power sharing. In this method, there is no need for a parametric model of the power system which is usually a problem in controller design in power systems. Instead, the measurement data has been used in the controller design process. In this method, there is no assumption on power feeders impedance such as dominantly inductive or dominantly resistive, which limits the generality of other methods. The proposed method can be applied to different control structures, i.e. centralized, distributed and decentralized during control design. The performance of the proposed method has been validated through simulation in a three-phase microgrid including synchronous generator, storage systems and PV units. The results show that this method can share reactive power among PV units while providing disturbance rejection in active power and voltage.

References

[1] J. Liang and K. Zhu, “Coded switching scheme for monitoring the operation of distribution capacitors,” *IEEE Transactions on Power Delivery*, vol. 33, no. 6, pp. 3075–3084, 2018.

[2] K. Diehl, J. A. Diaz de Leon, and M. Ghorai, “Applying svcs on distribution systems,” in *IEEE PES T D 2010*, 2010, pp. 1–7.

[3] D. B. Kulkarni and G. R. Udupi, “Ann-based svc switching at distribution level for minimal-injected harmonics,” *IEEE Transactions on Power Delivery*, vol. 25, no. 3, pp. 1978–1985, 2010.

[4] Jen-Hung Chen, Wei-Jen Lee, and Mo-Shing Chen, “Using a static var compensator to balance a distribution system,” *IEEE Transactions on Industry Applications*, vol. 35, no. 2, pp. 298–304, 1999.

[5] S. Ziaeinejad and A. Mehrizi-Sani, “Design tradeoffs in selection of the dc-side voltage for a d-statcom,” *IEEE Transactions on Power Delivery*, vol. 33, no. 6, pp. 3230–3232, 2018.

[6] C. Wang, X. Yin, Z. Zhang, and M. Wen, “A novel compensation technology of static synchronous compensator integrated with distribution transformer,” *IEEE Transactions on Power Delivery*, vol. 28, no. 2, pp. 1032–1039, 2013.

[7] S. Li, Y. Li, Y. Cao, Y. Tan, and B. Keune, “Capacity optimisation method of distribution static synchronous compensator considering the risk of voltage sag in high-voltage distribution networks,” *IET Generation, Transmission Distribution*, vol. 9, no. 16, pp. 2602–2610, 2015.

[8] S. Jain, M. B. Shadmand, and R. S. Balog, “Decoupled active and reactive power predictive control for pv applications using a grid-tied quasi-z-source inverter,” *IEEE Journal of Emerging and Selected Topics in Power Electronics*, vol. 6, no. 4, pp. 1769–1782, 2018.

[9] A. Micallef, M. Apap, C. Spiteri-Staines, J. M. Guerrero, and J. C. Vasquez, “Reactive power sharing and voltage harmonic distortion compensation of droop controlled single phase islanded microgrids,” *IEEE Transactions on Smart Grid*, vol. 5, no. 3, pp. 1149–1158, 2014.

[10] H. Han, Y. Liu, Y. Sun, M. Su, and J. M. Guerrero, “An improved droop control strategy for reactive power sharing in islanded microgrid,” *IEEE Transactions on Power Electronics*, vol. 30, no. 6, pp. 3133–3141, 2015.

[11] F. Valenciaga and C. A. Evangelista, “2-sliding active and reactive power control of a wind energy conversion system,” *IET Control Theory Applications*, vol. 4, no. 11, pp. 2479–2490, 2010.

[12] S. Bolognani, R. Carli, G. Cavraro, and S. Zampieri, “Distributed reactive power feedback control for voltage regulation and loss minimization,” *IEEE Transactions on Automatic Control*, vol. 60, no. 4, pp. 966–981, 2015.

[13] M. P. S. Gryning, Q. Wu, Kocewiak, H. H. Niemann, K. P. H. Andersen, and M. Blanke, “Stability boundaries for offshore wind park distributed voltage control,” *IEEE Transactions on Control Systems Technology*, vol. 25, no. 4, pp. 1496–1504, 2017.

[14] W. Meng, Q. Yang, and Y. Sun, “Guaranteed performance control of dfig variable-speed wind turbines,” *IEEE Transactions on Control Systems Technology*, vol. 24, no. 6, pp. 2215–2223, 2016.

[15] Y. Fan, G. Hu, and M. Egerstedt, “Distributed reactive power sharing control for microgrids with event-triggered communication,” *IEEE Transactions on Control Systems Technology*, vol. 25, no. 1, pp. 118–128, 2017.

[16] M. Todescato, J. W. Simpson-Porco, F. Dörfler, R. Carli, and F. Bullo, "Online distributed voltage stress minimization by optimal feedback reactive power control," *IEEE Transactions on Control of Network Systems*, vol. 5, no. 3, pp. 1467–1478, 2018.

[17] A. Karimi and C. Kammer, "A data-driven approach to robust control of multivariable systems by convex optimization," *Automatica*, vol. 85, pp. 227–233, 2017.

[18] C. Kammer and A. Karimi, "Decentralized and distributed transient control for microgrids," *IEEE Transactions on Control Systems Technology*, vol. 27, no. 1, pp. 311–322, 2019.

APPENDIX D

Synchrophasor-driven Control of Battery Energy Storage Systems for Frequency Control

Submitted to an IEEE Transactions Journal (2021)

Synchrophasor-driven Control of Battery Energy Storage Systems for Frequency Control

Dayan B. Rathnayake, *Student Member, IEEE,* Daniel Joseph Ryan, *Student Member, IEEE,* Reza Razzaghi, *Member, IEEE,* Alireza Karimi *Senior Member, IEEE,* and Behrooz Bahrani, *Senior Member, IEEE*

***Abstract*—Fast responding services, such as battery energy storage systems (BESSs), are increasingly getting deployed to deal with large frequency excursions that take place in low-inertia power systems. This paper proposes a novel wide area monitoring system based robust controller framework for BESSs to control the frequency in low-inertia grids. To overcome the modeling errors, this framework depends on an experimentally identified nonparametric model from synchrophasors. Further, an optimization-based robust fixed-structure control design method is adopted to tune the controller gains. The objective function, the infinity norm of the output sensitivity function, is minimized to enhance disturbance rejection while being subjected to performance constraints such as control effort and steady-state gain to achieve the required performance. The performance and efficacy of the proposed controller framework are validated through real-time hardware-in-the-loop experiments based on an Opal RT platform. The performance of the designed controller based on the framework is compared with that of a conventional droop controller for a variety of different cases.**

***Index Terms*—frequency stability, H_∞ control, low-inertia power systems, power system security, robust control**

I. Introduction

OWING to environmental obligations and thanks to the decreasing cost of renewable energy resources, many countries are actively transitioning toward low-carbon power systems. As a result, conventional fossil-fuel-driven synchronous power plants are getting displaced briskly by non-synchronous renewable energy sources (RESs), such as wind and solar. These RESs are typically tied to the electricity grid via power electronic converters. Hence, the rotating parts in these converter-tied generators (CTGs) are decoupled from the electricity grid by the power electronic converters. Therefore, the rapid displacement of synchronous power plants is causing a significant reduction of inertia in power systems. Consequently, the inertial response provided by synchronous generators following a contingency has decreased considerably. As a result, the frequency excursions that occur following a disturbance have become very high. One of the very first events to highlight the gravity of the challenges in CTGs abundant networks is the south Australian blackout in 2016 in which a dire initial rate of change of frequency (RoCoF) level of 6 Hz s^{-1} was recorded [1]. Therefore, as RESs become increasingly abundant in power systems, the need for fast-responding resources for frequency control has become urgent.

Various types of distributed energy resources are capable of providing fast frequency ancillary services in power systems with a high penetration of RESs. Virtual inertia provision from Type III and Type IV wind energy conversion systems is by far the most common type [2]. Similarly, solar photovoltaic systems can also be used to provide frequency support by rapidly injecting active power following a contingency [3]. Alternatively, an aggregation of smart loads can be utilized as a temporary power reserve subsequent to a fault [4]. In this paper, the use of battery energy storage systems (BESSs) for frequency control is investigated. Due to the emergence of issues caused by low-inertia levels [5], a rapidly growing interest is developing in using BESSs for frequency control in RES prolific grids [6]–[9]. BESSs are ideal to arrest high frequency excursions and to stabilize the system following contingencies due to their fast response rate, continuously reducing cost, and advancements in technology. However, the control strategies used in such BESSs to control frequency in low-inertia grids must be designed such that they are capable of working effectively under noise, uncertainties, and disturbances.

In the literature, there are a few standard control strategies that are used to control the BESSs. An outer loop active power droop is one of the simplest and most sought-after controllers in grid-supporting converters [10]. Its simplicity and satisfactory performance in a range of applications are its fortes. As an example, a power droop is used in practice in the Hornsdale power reserve in South Australia [11]. However, droop controllers suffer from a number of drawbacks such as poor transient performance, frequency deviations, unbalance harmonic current sharing, heavy reliance on output impedance, and not considering load dynamics [12]. Moreover, high droop gains are directly associated with stability issues of the system [13]. Further, it has been illustrated that to inject a burst of power during the first 500 ms following a fault, droop controller with a dead-band is improper for this purpose [14]. Therefore, in this paper, controllers are tuned based on an H_∞ technique to achieve robust stability and performance.

Conventional H_∞ control design for complex high-order systems such as the power system results in controllers of the same high-order as that of the system [15]. Generally, low-order controllers are preferred over high-order controllers, because they are easier to implement and are numerically more robust. Therefore, a fixed-structure control design method is used to design controllers of the desired order herein. An H_∞-based method to integrate storage systems to control the frequency is proposed in [16] and [17]. Although, [17] is for grid-forming converters in medium and low-voltage grids, both [16], [17] use parametric models to tune the controllers. Those models are prone to parametric uncertainities and modeling inaccuracies. Thus, their actual response differs from the theoretical response. Hence, in this paper, synchrophasors from wide area monitoring systems (WAMSs) are used to experimentally identify the frequency response of the system that is directly used in the control design.

Model identification in power systems is a widely investigated topic. Primarily, two main approaches exist in data-driven power system model identification. First approach is model identification through disturbances where model identification is done based on the step disturbances such as generator trippings, load trippings and line disconnections [20], [21] or using ambient data in normal operating conditions that are treated as stochastic white noise disturbances [18], [19]. One drawback of treating ambient data as stochastic white noise disturbances is that the data have to be recorded for a long time interval for this assumption to hold. Therefore, this paper followed the second approach of model identification, which uses a probing signal. In [22] and [23], a signal-injection-based method is used for experimentally identifying the reduced order model of the power system using a computationally intensive subspace state-space system identification (N4SID) method to tune power system stabilizers. In contrast, in this paper, a computationally efficient discrete-Fourier-transform-based method is used to identify the frequency response of the system.

A few references in the literature utilize WAMSs in fast frequency response applications. A wide area control strategy that distributes the weighted contingency size among the fast-acting resources in operation is proposed in [24]. An ancillary service allocation method based on the post contingency frequency nadir prediction from WAMS data is proposed in [25]. A targeted droop-enabled energy storage system dispatch method to limit the power flow change across the grid and to improve the energy storage system utilization is discussed in [26]. A significant shortcoming of these types of controllers is that closed-loop stability of the system is ignored in the design stage and only dealt with as a posterior condition. Therefore, in this paper, a novel wide area robust control framework that guarantees stability and optimal performance is proposed to control frequency in low-inertia grids using BESSs and WAMSs.

Contributions and merits of this paper are as follows:

1) a synchrophasor-driven frequency response identification method utilizing WAMSs is proposed. This method eliminates the need for prior knowledge of the power system and its components such as equipment and their configurations, topology, and operating conditions,
2) a novel framework that designs fixed-structure robust controllers for grid-supporting BESSs based on the experimentally identified frequency response is proposed, and
3) the efficacy of the proposed framework is validated in a real-time hardware-in-the-loop testbed that is equipped with a physical phasor measurement unit (PMU), thereby, practical aspects such as variable delays and uncertainties in the communication network are inherently taken into account.

The rest of the paper is structured as follows. Section II elaborates the proposed control framework, and Section III duly discusses the test power system used in this paper and the model identification. Section IV presents the optimization based H_∞ controller design and the convex formulation of the optimization problem. The performance validation of the proposed controller using real-time hardware-in-the-loop experimental data is presented in Section V. Finally, Section VI concludes the paper.

II. Wide area Robust Control Framework

As shown in Fig. 1, the control framework described in this paper proposes to take full advantage of the PMUs deployed in transmission networks. PMUs are promising sensing technology for control applications, such as the one described in this paper, for reasons such as providing complete system awareness, high sampling and reporting rates, and time-stamped data [27]. The control framework consists of two stages. First, the model of the plant is identified experimentally using the PMU data. To this end, the system is excited with a low-power active power injection, and the corresponding frequency variations are measured with PMUs. Then, the input-output data from all the BESSs are sent to an upstream phasor data concentrator (PDC) over Ethernet. Next, the input-output data is sent to a host PC for system-identification. Once the system-identification is finished, the control design stage starts. A key aspect of designing controllers in power systems is that they should be able to perform effectively in a wide range of conditions. To this end, the control design is formulated as an H_∞ control problem. Thus, robustness for uncertainties and stability for bounded disturbances can be achieved at the same time [29].

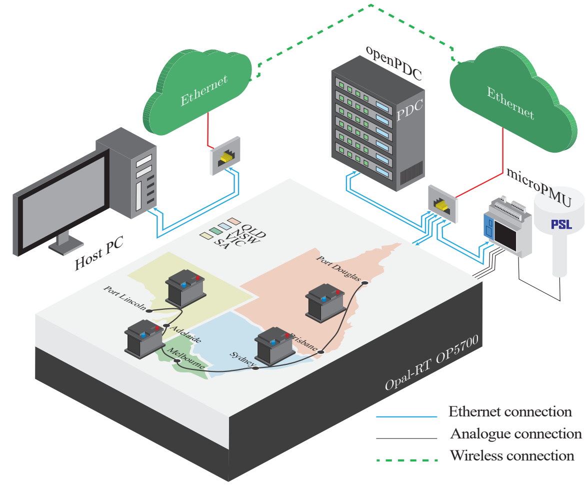

Fig. 1. Proposed control framework.

III. Power System Model Identification

In this section, first, the analyzed test power system is discussed. Next, the data-driven frequency-domain model identification method is presented. Finally, frequency-response data model of the linear time-invariant multi-input multi-output (LTI-MIMO) system from the power reference of the BESS to the frequency at the point of common coupling (PCC) is derived for the described test power system.

A. Test Power System

The studied power system in this paper is a multi-machine network that loosely resembles the south-eastern power system of Australia that comes under the National Electric Market (NEM). NEM is a long stringy network spanning for around 5000 km along the south-eastern seaboard of Australia. The testbed used in this paper is developed for designing and validating power system stabilizers (PSS) [30]. However, various versions of this testbed have been used for power system stability studies [31]. Since the focus of this paper is on low-inertia power systems, the network is augmented such that it becomes a RESs prolific power system. When augmenting the generation portfolio, different types of CTGs and their approximate locations are considered in order to be as close as it can be to the existing NEM network. The approximate locations of CTGs in the NEM are mapped into the network with the help of 16 zones of the national transmission network development plan (NTNDP) of Australian energy market operator (AEMO) [28]. The 16 zones of the NTNDP are mapped to the test system by considering the adjoining zones, the number of connections between areas, and the generation density of each zone. Furthermore, by mapping the 16 zones into the test system, it becomes easier to locate the corresponding renewable energy zones, which makes the integration of potential CTGs that could get connected in future seamless.

The augmented test power system used in this paper is shown in Fig. 2. When modeling the test power system, a wide range of technologies are considered for both synchronous and CTGs. For synchronous generation, coal power plants, combined cycle gas turbine (CCGT) generator plants and hydro-generator plants are considered. These synchronous power plants are modeled with governors, exciters, power system stabilizers, and fifth or sixth order synchronous machines. The coal power plants are modeled with steam turbine governors [32]. The IEEE turbine-governor model for CCGTs [33] is used for CCGTs, and hydraulic turbine-governor model [32] is used in hydropower plants.

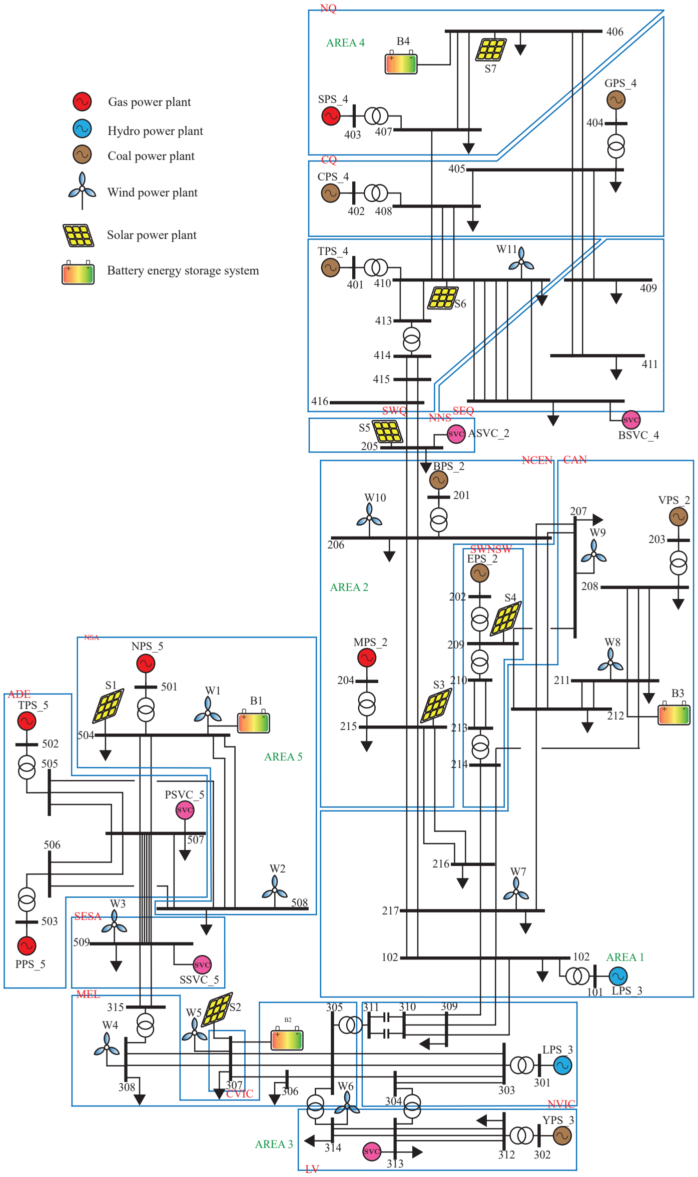

Fig. 2. Analyzed power system.

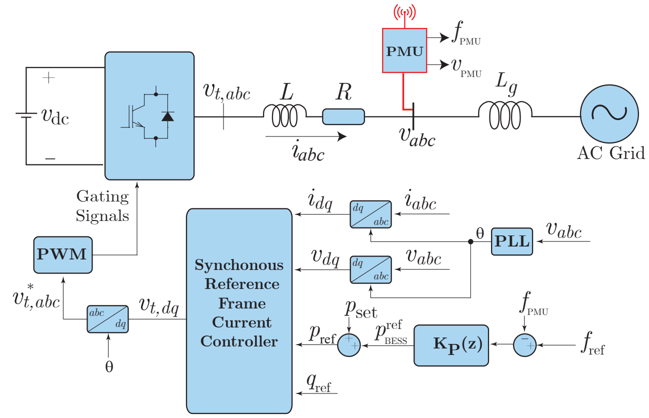

Fig. 3. BESS control structure.

TABLE I
GENERATION PORTFOLIO FOR >50% CTG PENETRATION.

Area	Load (MW)	Synchronous Generation Bus ID	$N_{\rm m}$	H (MWs)	$p_{\rm sync}$ (MW)	CTG Bus ID	$p_{\rm CTG}$ (MW)
4	4500	401	1	2.6	350	406	1920
		402	x	3.0	-	410	1920
		403	x	2.6	-		
		404	1	4.0	258		
Import from Area 4 to Area 2					-200		-
2	9550	201	x	3.2	-	206	2050
		202	1	2.8	500	207	2050
		203	1	2.6	375	211	2050
		204	1	3.2	492	217	2050
Import from Area 2 to Area 3 & 1					470		-
1&3	5950	101	1	3.6		307	1800
		301	1	2.8	600	308	1800
		302	x	3.5	-	314	900
Import from Area 1 & 3 to Area 5					200		-
5	2300	501	x	3.5	-	504	400
		502	1	4.0	200	508	1000
		503	x	7.5	-	509	400

As for CTGs, technologies such as wind farms, solar photovoltaics, and BESSs are considered. The electromagnetic effects and switching transients are assumed to be sufficiently fast, and CTGs and their controls are modeled to fit the time frame of the frequency variation dynamics [34]. As a means of simplification, a single aggregated wind turbine generator (WTG) or photovoltaic (PV) is modeled, and its MVA rating is scaled up by the number of in-service WTGs or PVs instead of modeling the whole wind or solar farm. This method of modeling is justified as effects from individual WTGs or PVs is of no interest in the conducted study.

Due to the superior performance over fixed speed wind farms, the majority of the recently installed wind farms are of Type IV wind farms. Also, in both Type III and Type IV wind farms, the rotating parts are decoupled from the grid. Therefore, the machine side is immune to disturbances coming from the grid. Type III and Type IV both behave similarly to frequency transients. Therefore, in this work, wind farms are modeled as fully rated converter based wind farms. The solar photovoltaics are modeled as grid-tied current-controlled converters. Similarly, the BESSs are modeled as grid-supporting converters coupled to a DC source. The converters are modeled as grid following current-controlled inverters with a closed-loop time constant of 2 ms. The control structure used in BESSs is shown in Fig. 3. The loads are modeled as constant impedance loads. In order to clearly quantify the contribution from BESSs towards frequency control, none of the CTGs participates in frequency control. Further, all the loads are considered to be static loads.

Since this paper is looking into low-inertia power systems, the generation mix is altered to have a significantly high CTG penetration. The generation portfolio for a 53% of CTG penetration level is given in Table I. The total demand of the system excluding the losses is 15.2 GW. The table shows the load in each area, data for each synchronous machine, and power output by CTGs at each bus. The number of active synchronous machines at each synchronous plant is given by $N_{\rm m}$ where x indicates that no machines are active in the corresponding power plant. The H column represents the corresponding inertia constants. The rest of the parameters for synchronous machines, transmission lines, transformers, static var compensators (SVCs) can be found in [30]. The total active power supplied by the synchronous machines amounts to 7003.2 MW while that of CTGs is 8395 MW. Table I also presents the imports from and to each area under synchronous imports ($p_{\rm sync}$) column since all the regions are connected with AC connections.

B. Wide Area Monitoring System

In the proposed control framework, WAMSs are leveraged to get an accurate reading of the frequency from multiple points in the power system to, first, identify the frequency-response data model of the LTI-MIMO plant and, then, to control the BESSs. In this test power system, four PMUs, each connected to the BESSs' point of connection, are used. To authors' best of knowledge, most of the literature that utilize WAMS in their control loops have not tested their controllers with actual PMUs. Many of them use a primitive simulation model for PMUs [35]. Therefore, in this work, a WAMS with an actual PMU and three other simulation models of PMUs are used to validate the findings. To this end, a Power Standards Lab's microPMU [36] is used as the physical PMU. The other three are modeled as simulation PMU models based on the enhanced interpolated discrete Fourier transform that is shown to perform well under steady-state as well as transient conditions [37].

As shown in Fig. 1, as per the framework, the synchrophasors from PMUs are transmitted via PDCs to a host computer for identification and control stages. The PDCs are used to aggregate the PMU data from local PMUs and stream them for further processing. In this paper, the PDC is modeled using openPDC [38]. The PDC is configured to receive synchrophasors from the four PMUs, and the output streams are set to transmit the frequency measurements. The transmission control protocol (TCP) and user datagram protocol (UDP) are the two widely used protocols for PMU data transmission over Ethernet. Due to the lack of acknowledgment process, UDP is much faster than TCP. Therefore, in this work, UDP is preferred over TCP to transmit the PMU data over the Ethernet.

In this paper, the PMU data is transmitted over the legacy Ethernet network of the university. Thus, uncertainties and variable time delays due to network congestion are inevitably taken into account. In order to overcome the variable time delays, a circular buffer mechanism is used to buffer five data samples (to take into consideration the maximum observed delay of the Ethernet network) before feeding into the controller. Hence, the resulting data stream is an evenly sampled feedback signal that can be used for identification and control purposes. The synchrophasor streams of the PMUs are according to the IEEE C37.118 standard [39]. The reporting rate of all four of the PMUs is set to be 10 ms.

C. Data-Driven Model Identification

In order to design controllers for BESSs, first, the model of the plant must be derived. The model of the plant can be derived either based on the physics of the system or experimentally. Since no real system can be mathematically modeled precisely, models based on the physics of the system end up being less accurate due to unmodeled dynamics and parameter uncertainties. Therefore, in this paper, an experimentally identified nonparametric model of the plant is used to design the controllers. One of the main advantages of experimentally identifying the model of the plant is that no prior knowledge is required regarding the generators, lines, loads, and other equipment in the system.

The data-driven controller design framework proposed in this paper comprises two stages. The first stage is identifying the frequency response data model of the LTI-MIMO system (G), which is represented by

$$\begin{bmatrix} F_{\text{PMU},1} \\ \vdots \\ F_{\text{PMU},n} \end{bmatrix} = \underbrace{\begin{bmatrix} G_{1,1} & \dots & G_{1,m} \\ \vdots & \ddots & \vdots \\ G_{n,1} & \dots & G_{n,m} \end{bmatrix}}_{G} \begin{bmatrix} P^{\text{ref}}_{\text{BESS},1} \\ \vdots \\ P^{\text{ref}}_{\text{BESS},m} \end{bmatrix} \tag{1}$$

in which F_{PMU} and $P^{\text{ref}}_{\text{BESS}}$ are local frequency and active power reference of the BESSs, respectively, *m* is the number of inputs, and *n* is the number of outputs.

In order to estimate the frequency domain model of G, the system is stimulated by superimposing a signal over the $p^{\text{ref}}_{\text{BESS}}$. Then, the resulting variations in the frequency of interest are monitored through PMUs. Although different signals can be used to excite the system, in this paper, a maximum length pseudo-random binary sequence (PRBS) as shown in Fig. 4 is used as the excitation signal. The PRBS is a periodic signal that toggles between two constant levels around zero and has a flat spectrum similar to discrete white noise. A b-bit maximum length PRBS signal can be synthesized using a b-bit shift register that shifts one bit at each sampling time (T_{s}), with feedback of exclusive-OR operation performed between two specific bits [41]. The data length of a single period PRBS signal (d) is given by

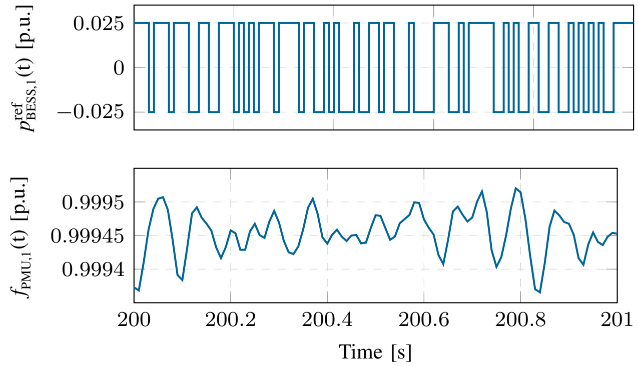

Fig. 4. One second of the injected 10-bit PRBS signal and the corresponding frequency signal.

$$d = 2^b - 1, \tag{2}$$

where b is the number of bits. Since there are multiple BESSs, each BESS should excite the system only after the excitations of all the other BESSs are finished. Ideally, for identification purposes, injecting one single period of PRBS is enough. However, this results in a higher noise content, especially in the high-frequency range of the identified model of the plant. Therefore, multiple periods of the PRBS are injected to reduce the effect of noise sources [41]. If the excitation of one BESS is called an experiment, in each experiment, *r* number of periods of PRBS are used. The selection of the magnitude of the PRBS signal (α) is entirely up to the designer. However, the chosen value for α should not be too large to cause disruptions nor severe power quality issues in normal operating conditions. The values used for the parameters of PRBS are given in Table II.

If the system is excited by the m^{th} BESS, and input ($u_m \in \mathbb{R}^{d\times 1}$) and output data are gathered, each corresponding $\hat{G}_{k,m}(j\omega) \in \mathbb{C}^{n\times m}$ $k = 1, \cdots, n$ frequency response data model can be identified by

$$\hat{G}_{k,m}(j\omega) = \frac{\left[\sum_{i=1}^{r} \mathcal{F}_i\left\{y_{k,i}\right\}\right]/r}{\mathcal{F}\left\{u_m\right\}} \quad \forall\omega \in \Omega \tag{3}$$

in which $\mathcal{F}\{.\}$ stands for discrete Fourier transform (DFT), and $y_{k,i} \in \mathbb{R}^{d\times 1}$ corresponds to the i^{th} repetition of the frequency from the k^{th} PMU. Furthermore, Ω is a finite set of frequencies, and it is defined as $\Omega = \{\omega_N = \dfrac{N\pi}{dTs} | N = 0, \cdots, d\}$. As it can be seen in (3), the Fourier coefficients of each repetition of the PMU frequency is averaged to eliminate the effect of noise. Note that, alternatively, the *etfe()* command in system identification toolbox in MATLAB provides equal results.

As shown in Fig. 2, in this study, four BESSs and four PMUs connected to BESSs' PCCs are used. Therefore, $\hat{G}(j\omega)$ becomes a 4×4 frequency-response data model. Due to the page limitation, not all 16 frequency responses are shown. However, Fig. 5 shows the identified frequency domain model from active power reference

TABLE II
PRBS PULSE STREAM DATA

Parameter	Value
Magnitude of the PRBS pulse (α)	5 MW
Identification sampling time (T_s)	10 ms
Number of bits (b)	10
Data length of a single period PRBS (d)	1023
Number of repetitions (r)	5

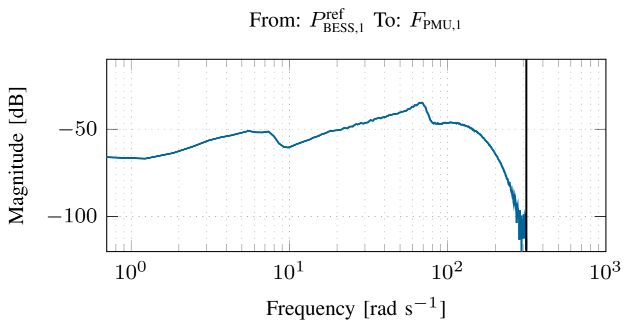

Fig. 5. Frequency response of the active power reference to frequency of battery 1 connected at bus 501.

to the PMU frequency of the BESS connected to bus 501. The identified frequency range spans from 0 to 314.16 rad s^{-1} with a linear spacing of 0.307 rad s^{-1}.

IV. Optimization Based Controller Design

Once the frequency-response data model of the power system is identified, the robust controller design can be done such that the controlled signals achieve the desirable characteristics under noise, disturbances, and uncertainties. In this section, the optimization-based controller design is explained.

A. Controller Structure

In this paper, a fixed-structure discrete-time transfer function is chosen as the controller structure. The discrete-time control strategy can be presented as

$$\begin{bmatrix} P^{\text{ref}}_{\text{BESS},1}(z) \\ \vdots \\ P^{\text{ref}}_{\text{BESS},m}(z) \end{bmatrix} = K(z) \begin{bmatrix} F_{\text{ref}}(z) - F_{\text{PMU},1}(z) \\ \vdots \\ F_{\text{ref}}(z) - F_{\text{PMU},n}(z) \end{bmatrix} \tag{4}$$

in which $K(z) = X(z) \cdot Y(z)^{-1}$ where

$$X(z) = \sum_{i=0}^{p} \mathcal{X}_{(p-i)} \cdot z^{-i}, \tag{5}$$

$$Y(z) = I + \sum_{j=1}^{q} \mathcal{Y}_{(q-j)} \cdot z^{-j} \tag{6}$$

for any control structure and $F_{\text{ref}}(z)$ is the frequency reference. Since decentralized controllers are designed in this paper, the $(k,l)^{\text{th}}$ element of $\mathcal{X}_{(p-i)} \in \mathbb{R}^{m\times n}$ and $\mathcal{Y}_{(q-j)} \in \mathbb{R}^{n\times n}$ are chosen to be as

$$\mathcal{X}_{(p-i)}(k,l) = \begin{cases} x^{k,l}_{(p-i)}, & \text{for } k = l \\ 0, & \text{for} k \neq l \end{cases} \tag{7}$$

and

$$\mathcal{Y}_{(q-j)}(k,l) = \begin{cases} y^{k,l}_{(q-j)}, & \text{for } k = l \\ 0, & \text{for } k \neq l \end{cases}. \tag{8}$$

The parameters $x^{k,l}_{(p-i)}$, $i = 0, \cdots, p$ and $y^{k,l}_{(q-j)}$, $j = 0, \cdots, q$ are the respective numerator and denominator controller gains of the $(k,l)^{\text{th}}$ controller that are tuned during the optimization stage. The values $p, q \in \mathbb{Z}^+$ are strictly selected by the designer, allowing them to design low-order controllers as opposed to conventional robust control design methods where designing controllers for high-order plants is challenging. For the sake of clarity in notation, hereafter in the discussion, the terms such as z, $e^{j\omega}$, s and $j\omega$ are removed from the transfer functions and the identity matrix is represented by I.

B. Control Specifications

In order to make the closed-loop system output (frequency) immune to disturbances caused by power fluctuations, the output sensitivity function ($\mathcal{S}$) is appropriately shaped. The performance of the controller is achieved by defining performance specifications such as disturbance rejection performance, frequency control performance, and steady-state gain requirements as constraints in the frequency domain. The following sections explain how the conventional control specifications such as bandwidth and damping are achieved in terms of constraints in the frequency domain.

1) Disturbance Rejection Performance: The control objective considered in this paper is to minimize the impact on system frequency caused by contingencies such as load changes and generators tripping. To this end, disturbance rejection by minimizing the H_∞ norm of $\mathcal{S}$ is considered. $\mathcal{S} = (I + GK)^{-1}$ is the transfer function from external disturbances to the process output of system frequency. Therefore, as it is shown by

$$\min_K \|W_1 \mathcal{S}\|_\infty, \tag{9}$$

the infinity norm of the weighted sensitivity is minimized over the frequency range. In (9), W_1 is a weighting filter that is used to facilitate the sensitivity function to satisfy certain frequency domain specifications such as bandwidth (ω_b) and peak sensitivity (M_s). A suitable practical transfer function for this purpose is

$$W_1 = \left(\frac{s/\sqrt[\lambda]{M_s} + \omega_b}{s + \omega_b \sqrt[\lambda]{\varepsilon}} \right)^\lambda \cdot I, \tag{10}$$

where ε is the acceptable steady-state error for a step disturbance, and a steeper roll-off between low-frequency and high-frequency can be achieved by increasing the value of $\lambda \in \mathbb{Z}^+$ [42].

2) Frequency Control Performance: In order to manage the effect of disturbance on control input, input sensitivity function $\mathcal{U}$ can be considered. $\mathcal{U} = K\mathcal{S}$ is the transfer function from frequency disturbances to the control input. To this end, the constraint

$$\|W_2\, \mathcal{U}\|_\infty < 1 \tag{11}$$

is considered. In (11), W_2 is a weighting filter that is used to fulfil design requirements such as controller bandwidth (ω_{bc}) and peak sensitivity (M_u). A suitable practical transfer function for this purpose is

$$W_2 = \left(\frac{s + \omega_{bc}/\sqrt[\rho]{M_u}}{\sqrt[\rho]{\varepsilon_1} s + \omega_{bc}} \right)^\rho \cdot I, \tag{12}$$

where ε_1 is the acceptable steady-state error for a step disturbance, and a steeper roll-off between low-frequency and high-frequency can be achieved by increasing the value of $\rho \in \mathbb{Z}^+$ [42].

3) Steady-State Gain: Steady-state gain (K_{ss}) represents the DC gain of the controller. It can be expressed as a constraint in the frequency domain by considering the gain of K at $\omega = 0$. To this end, the constraint

$$\left[\sum_{i=0}^{p} \mathcal{X}_{(p-i)} \right] \cdot \left[I + \sum_{j=1}^{q} \mathcal{Y}_{(q-j)} \right]^{-1} = K_{\text{ss}} \tag{13}$$

TABLE III
DATA USED FOR THE EXPERIMENTAL VALIDATION

Parameter	Value
W_1	ω_b=500, M_s=1.1,ε=1, λ=2
W_2	ω_{bc}=10000,M_u=800,ε_1=50, ρ=2
K_{ss}	diag(100 100 100 100)
p,q	5,5
K_c	diag(33 33 33 33)

is considered. This constraint can be used to achieve steady-state active power sharing enabling the BESSs to share the active power based on their rating.

C. Convex Optimization Problem Formulation

The optimization problem described in Section IV-B is nonconvex. Therefore, a method to convert it to a convex optimization problem is proposed in [40]. In [40], it is described how the constraints can be approximated by an inner-convex approximation. First, the constraints are reformulated as a set of convex-concave constraints. Next, the concave terms are linearized around an initial controller ($K_c = X_c Y_c^{-1}$) using the Taylor expansion. Finally, using the Shur complement, the constraints can be portrayed as a set of linear matrix inequalities (LMIs). The complete convex optimization problem can be summarized as

$$\min_{X,Y} \quad \gamma \tag{14a}$$

$$\text{s.t.} \quad \begin{bmatrix} \gamma I & W_1 Y \\ (W_1 Y)^* & J^* J_c + J_c^* J - J_c^* J_c \end{bmatrix} > 0 \quad \forall \omega \in \Omega, \tag{14b}$$

$$\begin{bmatrix} I & W_2 X \\ (W_2 X)^* & J^* J_c + J_c^* J - J_c^* J_c \end{bmatrix} > 0 \quad \forall \omega \in \Omega, \tag{14c}$$

$$\textstyle\sum_{i=0}^{p} \mathcal{X}_{(p-i)} - K_{ss} \left[I + \sum_{j=1}^{q} \mathcal{Y}_{(q-j)} \right] = 0, \tag{14d}$$

$$Y^* Y_c + Y_c^* Y - Y_c^* Y_c > 0 \quad \forall \omega \in \Omega \tag{14e}$$

where γ is an upper bound on the infinity norm of the $W_1\mathcal{S}$, $J = (Y + GX)$, $J_c = (Y_c + GX_c)$, and $\{\}^*$ denotes the conjugate transpose operation. Minimizing γ under constraint (14b) is for the objective function. Similarly, constraint (14c) is for the control effort. The equality (14d) indicates the constraint on steady-state gain of the controllers. Finally, the constraint (14e) is for the stability of the closed-loop system. As it is shown in the optimization problem, these constraints are evaluated at each frequency of the set Ω. One drawback of this method is that a suboptimal controller that is far from the control specifications could be obtained as a result of the inner approximation made of the original optimization problem. In order to circumvent this problem, the optimization problem is solved iteratively by using the suboptimal controller of the last iteration as the initial controller for the next iteration. Thus, the solution converges to a local optimum of the original problem. A flowchart is given in Fig. 6 to aid the reader to understand the complete synchrophasor-driven control framework proposed in this paper.

The optimization problem discussed above is formulated using Yalmip [43] and solved using MOSEK [44]. The p and q values are chosen to be 5. A droop controller of 0.03 p.u. is chosen as the initial controller, and the W_1 and W_2 filter values are given in Table III. Fig. 7 shows the reduction of maximum singular value of the output sensitivity over the frequency range for the designed controller and initial droop controller. $\mathcal{S}_{\mathrm{Kc}}$ represents the maximum singular value of the output sensitivity when a droop controller is used. $\mathcal{S}_{\mathrm{K}}$ represents the maximum singular value of the output sensitivity over the frequency range with the designed controller. In Fig. 7, it is clearly shown that the maximum singular value of the

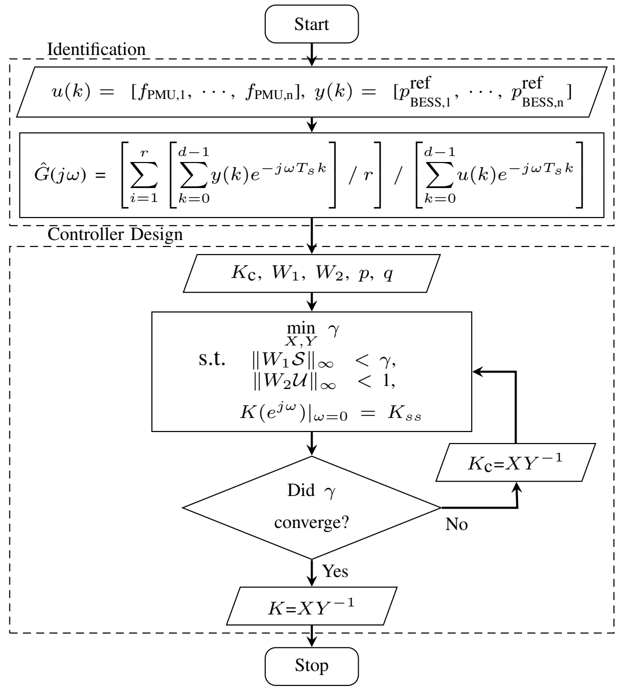

Fig. 6. Proposed wide area control framework flowchart.

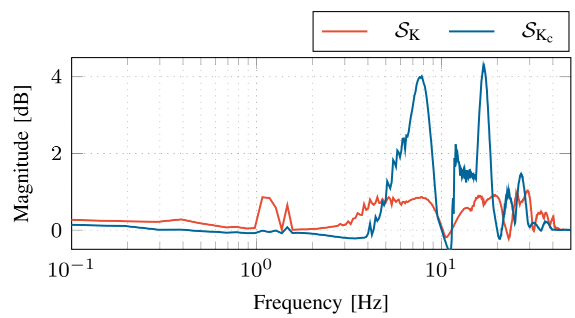

Fig. 7. Minimization of maximum output sensitivity over the frequency range. $\mathrm{S_{Kc}}$ represents the maximum output sensitivity with a 3% droop controller, and $\mathrm{S_K}$ represents the maximum output sensitivity with the designed controller.

output sensitivity is reduced from 4.28 dB to 1.02 dB with the newly designed controller. The maximum singular value of the output sensitivity function directly correlates with the damping. Therefore, damping is considerably increased by the newly designed controller by reducing the maximum singular value of the output sensitivity function.

V. REAL-TIME HARDWARE-IN-THE-LOOP TESTING

The test power system described in Section III is modeled in Opal-RT's real-time simulation platform (RT-LAB) and simulated on a real-time simulator (OP5700) to validate the performance of the designed controllers through non-linear simulations. As described before, a microPMU from PSL is used as the actual PMU, and the openPDC is used as the PDC for the PMU data transmission. The common university communication network is used to send the PMU data over Ethernet instead of any dedicated communication channels.

A. Controller Performance Evaluation

The controller performance is quantified through the following two indices 1) frequency nadir and 2) quasi-steady-state frequency (QSSF). The center of inertia frequency (f_{coi}) of the system is used to retrieve the frequency nadir and QSSF. f_{coi} is utilized as a means

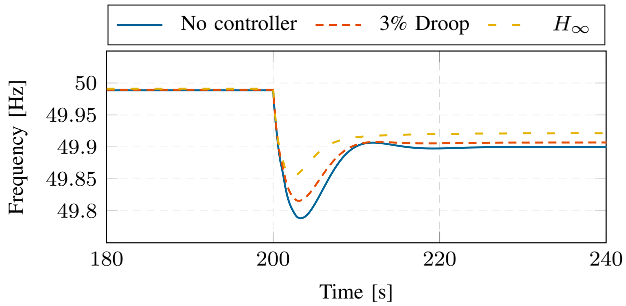

Fig. 8. Frequency trajectories for a load change of 360 MW. Blue, red, and yellow graphs represent the cases no controller, 3% droop controller and designed H_∞ controller, respectively.

of considering a unique frequency for the whole system subsequent to a disturbance. f_{coi} can be calculated by

$$f_{\text{coi}} = \frac{\sum_{i=1}^{N_T} H_i \cdot f_{\text{rot},i}}{\sum_{i=1}^{N_T} H_i}, \tag{15}$$

where H_i and $f_{\text{rot},i}$ are the inertia constant and the rotor speed of the i^{th} synchronous machine in the system, respectively. N_T is the total number of synchronous machines active in the system.

The controller performance is tested for two types of disturbances: 1) a sudden load change and 2) a generator disconnection. The resulting frequency trajectories with the H_∞ controller for both types of disturbances are compared with the frequency trajectories with a droop controller. A droop coefficient of 3% is considered for the droop controller as droop coefficients higher than this cause the simulation to become unstable. The frequency trajectories without any controller are provided for both types of disturbances to clearly distinguish the improvement due to the H_∞ controller. In both disturbance scenarios, the power ratings of SA and VIC batteries are 100 MW each, respectively, whereas those of NSW and QLD batteries are 200 MW each, respectively.

B. Scenario 1: Load Change

The objective of this type of scenario is to reject the frequency disturbance and maintain the system frequency within the statutory limits. In this scenario, a static load of size 360 MW is connected to busbar 217 at $t = 200$ s. In Fig. 8, the frequency trajectories for the three cases of no controller, droop controller, and the designed H_∞ controller are shown.

As shown in Fig. 8, the proposed controller improves the frequency nadir from 49.79 Hz to 49.85 Hz by 0.06 Hz as opposed to the droop controller for which the improvement is only from 49.79 Hz to 49.82 Hz. The QSSF also is improved with the H_∞ controller from 49.9 Hz to 49.92 Hz in contrast with the improvement from 49.9 Hz to 49.91 Hz with the droop controller.

Since fast frequency control is a power-oriented task, the active power output of each battery is of prime importance. Fig. 9 shows the active power output of each four batteries that are responding to the load change.

Since the rating of P_{NSW} and P_{QLD} is twice as the rating of P_{SA} and P_{VIC}, it can be seen the power output increment of P_{NSW} and P_{QLD} is twice as much as P_{SA} and P_{VIC}. The active power output increments of P_{SA} and P_{VIC} are 13.95 MW and 13.98 MW whereas the active power output increments of P_{NSW} and P_{QLD} are 28.05 MW and 27.8 MW, respectively.

C. Scenario 2: Generator Disconnection

As the next case, a generator disconnection scenario is considered. To this end, a generator of size 260 MW that is connected to busbar 209 is disconnected at $t = 200$ s. The frequency trajectories for the three cases of no controller, droop controller, and the designed H_∞ controller are shown in Fig. 10.

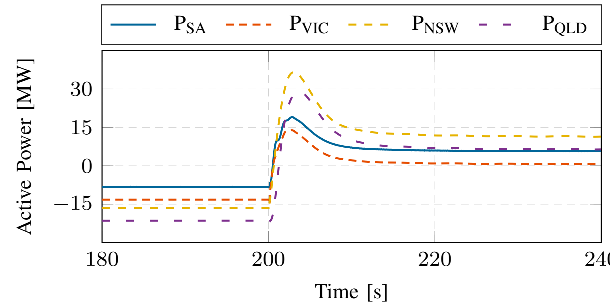

Fig. 9. Battery active power change for a load change of 360 MW. Blue, red, yellow, and purple graphs represent the active power output of P_{SA}, P_{VIC}, P_{NSW} and P_{QLD} with the designed H_∞ controller, respectively.

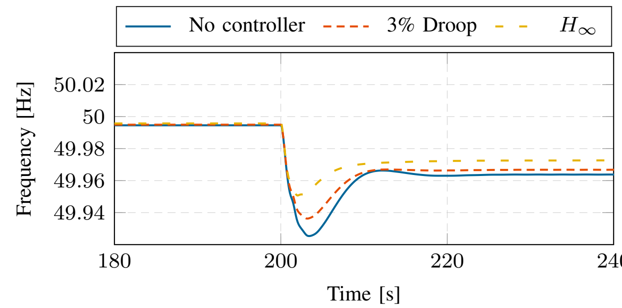

Fig. 10. Frequency trajectories for a generator trip of 260 MW. Blue, red, and yellow graphs represent the cases no controller, 3% droop controller and designed H_∞ controller, respectively.

As shown in Fig.10, the proposed controller improves the frequency nadir from 49.93 Hz to 49.95 Hz by 0.02 Hz as opposed to the droop controller for which the improvement is only from 49.93 Hz to 49.94 Hz. The QSSF is also improved with the H_∞ controller from 49.963 Hz to 49.973 Hz. In comparison, the improvement with the droop controller is only from 49.963 Hz to 49.967 Hz. Fig. 11 shows the active power output of each four batteries responding to the generator disconnection.

Similar to the load change scenario, due to the equal frequency bias chosen, the power increments of P_{NSW} and P_{QLD} batteries are twice as much as P_{SA} and P_{VIC} batteries. The power increments of P_{SA} and P_{VIC} are 4.69 MW and 4.63 MW as opposed to 9.26 MW and 9.3 MW, which are power increments of P_{NSW} and P_{QLD}, respectively.

VI. Conclusions

Rapid displacement of synchronous machines by RES has made a convincing case for fast-reacting resources such as BESSs. This paper proposes a novel robust control design framework based on synchrophasor-data for frequency control using grid-supporting BESSs in the transmission network. The framework consists of two parts. First, the synchrophasor-data-driven frequency response data model of the LTI-MIMO system identification stage that overcomes the difficulties in parametric model-based methods is utilized. Next, an H_∞ based fixed-structure controller design method based on convex optimization is used for the control design stage. The experimental results have corroborated the superior performance of proposed controllers using a real-time hardware-in-the-loop testbed. In future works, distributed controller design utilizing communication between neighborhood batteries will be explored. Furthermore, multi-model uncertainty resulting from different operating points will be investigated.

Acknowledgment

The authors would like to thank Jingwen Ding for their input in PMU modeling.

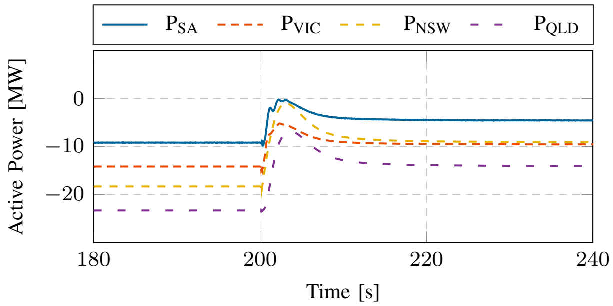

Fig. 11. Battery active power change for a generator trip of 260 MW. Blue, red, yellow, and purple graphs represent the active power output of P_{SA}, P_{VIC}, P_{NSW} and P_{QLD} with the designed H_∞ controller, respectively.

References

[1] AEMO, "Black System South Australia 28 September 2016", Tech. Rep. 2017 March.

[2] J. Ekanayake and N. Jenkins, "Comparison of the response of doubly fed and fixed-speed induction generator wind turbines to changes in network frequency," in IEEE Transactions on Energy Conversion, vol. 19, no. 4, pp. 800-802, Dec. 2004, doi: 10.1109/TEC.2004.827712.

[3] A. F. Hoke, M. Shirazi, S. Chakraborty, E. Muljadi and D. Maksimovic, "Rapid Active Power Control of Photovoltaic Systems for Grid Frequency Support," in IEEE Journal of Emerging and Selected Topics in Power Electronics, vol. 5, no. 3, pp. 1154-1163, Sept. 2017, doi: 10.1109/JESTPE.2017.2669299.

[4] A. Molina-García, F. Bouffard and D. S. Kirschen, "Decentralized Demand-Side Contribution to Primary Frequency Control," in IEEE Transactions on Power Systems, vol. 26, no. 1, pp. 411-419, Feb. 2011, doi: 10.1109/TPWRS.2010.2048223.

[5] F. Milano, F. Dörfler, G. Hug, D. J. Hill and G. Verbič, "Foundations and Challenges of Low-Inertia Systems (Invited Paper)," 2018 Power Systems Computation Conference (PSCC), Dublin, 2018, pp. 1-25, doi: 10.23919/PSCC.2018.8450880.

[6] J. W. Shim, G. Verbič, N. Zhang and K. Hur, "Harmonious Integration of Faster-Acting Energy Storage Systems Into Frequency Control Reserves in Power Grid With High Renewable Generation," in IEEE Transactions on Power Systems, vol. 33, no. 6, pp. 6193-6205, Nov. 2018.

[7] L. Toma et al., "On the virtual inertia provision by BESS in low inertia power systems," 2018 IEEE International Energy Conference (ENERGYCON), Limassol, 2018, pp. 1-6.

[8] S. M. Alhejaj and F. M. Gonzalez-Longatt, "Investigation on grid-scale BESS providing inertial response support," 2016 IEEE International Conference on Power System Technology (POWERCON), Wollongong, NSW, 2016, pp. 1-6.

[9] F. M. Gonzalez-Longatt and S. M. Alhejaj, "Enabling inertial response in utility-scale battery energy storage system," 2016 IEEE Innovative Smart Grid Technologies - Asia (ISGT-Asia), Melbourne, VIC, 2016, pp. 605-610.

[10] J. Rocabert, A. Luna, F. Blaabjerg and P. Rodríguez, "Control of Power Converters in AC Microgrids," in IEEE Transactions on Power Electronics, vol. 27, no. 11, pp. 4734-4749, Nov. 2012, doi: 10.1109/TPEL.2012.2199334.

[11] AURECON "Large-Scale Battery Storage Knowledge Sharing Report", Tech. Rep. 2019 November.

[12] J. M. Guerrero, L. Hang and J. Uceda, "Control of Distributed Uninterruptible Power Supply Systems," in IEEE Transactions on Industrial Electronics, vol. 55, no. 8, pp. 2845-2859, Aug. 2008, doi: 10.1109/TIE.2008.924173.

[13] I. Chung, W. Liu, D. A. Cartes, E. G. Collins and S. Moon, "Control Methods of Inverter-Interfaced Distributed Generators in a Microgrid System," in IEEE Transactions on Industry Applications, vol. 46, no. 3, pp. 1078-1088, May-june 2010, doi: 10.1109/TIA.2010.2044970.

[14] P. V. Brogan, R. Best, D. J. Morrow, C. Bradley, M. Rafferty and M. Kubik, "Triggering BESS Inertial Response with Synchronous Machine Measurements," 2018 IEEE Power & Energy Society General Meeting (PESGM), Portland, OR, 2018, pp. 1-5.

[15] J. C. Doyle, K. Glover, P. P. Khargonekar and B. A. Francis, "State-space solutions to standard H/sub 2/ and H/sub infinity / control problems," in IEEE Transactions on Automatic Control, vol. 34, no. 8, pp. 831-847, Aug. 1989, doi: 10.1109/9.29425.

[16] D. Zhu and G. Hug-Glanzmann, "Coordination of storage and generation in power system frequency control using an H_∞ approach," in IET Generation, Transmission & Distribution, vol. 7, no. 11, pp. 1263-1271, November 2013, doi: 10.1049/iet-gtd.2012.0522.

[17] C. Kammer and A. Karimi, "Decentralized and Distributed Transient Control for Microgrids," in IEEE Transactions on Control Systems Technology, vol. 27, no. 1, pp. 311-322, Jan. 2019, doi: 10.1109/TCST.2017.2768421.

[18] K. Tuttelberg, J. Kilter, D. Wilson and K. Uhlen, "Estimation of Power System Inertia From Ambient Wide Area Measurements," in IEEE Transactions on Power Systems, vol. 33, no. 6, pp. 7249-7257, Nov. 2018, doi: 10.1109/TPWRS.2018.2843381.

[19] P. Huynh, H. Zhu, Q. Chen and A. E. Elbanna, "Data-Driven Estimation of Frequency Response From Ambient Synchrophasor Measurements," in IEEE Transactions on Power Systems, vol. 33, no. 6, pp. 6590-6599, Nov. 2018, doi: 10.1109/TPWRS.2018.2832838.

[20] G. Chavan, M. Weiss, A. Chakrabortty, S. Bhattacharya, A. Salazar and F. Ashrafi, "Identification and Predictive Analysis of a Multi-Area WECC Power System Model Using Synchrophasors," in IEEE Transactions on Smart Grid, vol. 8, no. 4, pp. 1977-1986, July 2017, doi: 10.1109/TSG.2016.2531637.

[21] P. M. Ashton, C. S. Saunders, G. A. Taylor, A. M. Carter and M. E. Bradley, "Inertia Estimation of the GB Power System Using Synchrophasor Measurements," in IEEE Transactions on Power Systems, vol. 30, no. 2, pp. 701-709, March 2015, doi: 10.1109/TPWRS.2014.2333776.

[22] Ning Zhou, J. W. Pierre and J. F. Hauer, "Initial results in power system identification from injected probing signals using a subspace method," in IEEE Transactions on Power Systems, vol. 21, no. 3, pp. 1296-1302, Aug. 2006.

[23] I. Kamwa, G. Trudel and L. Gerin-Lajoie, "Low-order black-box models for control system design in large power systems," Proceedings of Power Industry Computer Applications Conference, Salt Lake City, UT, USA, 1995, pp. 190-198

[24] Q. Hong et al., "Design and Validation of a Wide Area Monitoring and Control System for Fast Frequency Response," in IEEE Transactions on Smart Grid, doi: 10.1109/TSG.2019.2963796.

[25] C. Lai and C. Liu, "A Scheme to Mitigate Generation Trip Events by Ancillary Services Considering Minimal Actions of UFLS," in IEEE Transactions on Power Systems, doi: 10.1109/TPWRS.2020.2993449.

[26] Cai, L., et al. (2019). "A Test Model of a Power Grid With Battery Energy Storage and Wide-Area Monitoring." IEEE Transactions on Power Systems 34(1): 380-390.

[27] L. G. Meegahapola, S. Bu, D. P. Wadduwage, C. Y. Chung and X. Yu, "Review on Oscillatory Stability in Power Grids with Renewable Energy Sources: Monitoring, Analysis, and Control using Synchrophasor Technology," in IEEE Transactions on Industrial Electronics, doi: 10.1109/TIE.2020.2965455.

[28] AEMO, "National Transmission Network Development Plan 2015", Tech Rep. 2015 Nov.

[29] K. Zhou, J.C. Doyle and K. Glover, Robust and optimal control, Prentice-Hall, 1995.

[30] M. Gibbard and D. Vowles, "Simplified 14-generator model of the SE Australian power system", The University of Adelaide, Tech. Rep. Jul, 2010.

[31] A. S. Ahmadyar, S. Riaz, G. Verbič, A. Chapman and D. J. Hill, "A Framework for Assessing Renewable Integration Limits With Respect to Frequency Performance," in IEEE Transactions on Power Systems, vol. 33, no. 4, pp. 4444-4453, July 2018, doi: 10.1109/TPWRS.2017.2773091.

[32] I. C. Report, "Dynamic Models for Steam and Hydro Turbines in Power System Studies," in IEEE Transactions on Power Apparatus and Systems, vol. PAS-92, no. 6, pp. 1904-1915, Nov. 1973.

[33] "Dynamic models for combined cycle plants in power system studies," in IEEE Transactions on Power Systems, vol. 9, no. 3, pp. 1698-1708, Aug. 1994.

[34] G. De Carne et al., "Which Deepness Class Is Suited for Modeling Power Electronics?: A Guide for Choosing the Right Model for Grid-Integration Studies," in IEEE Industrial Electronics Magazine, vol. 13, no. 2, pp. 41-55, June 2019.

[35] S. A. R. Konakalla, A. Valibeygi and R. A. de Callafon, "Microgrid Dynamic Modeling and Islanding Control With Synchrophasor Data," in IEEE Transactions on Smart Grid, vol. 11, no. 1, pp. 905-915, Jan. 2020.

[36] Power Standards Lab, *microPMU*, Power Standards Lab, 980 Atlantic Ave., Alameda, California 94501. Accessed on April 04th, 2020. [Online] Available: https://www.powerstandards.com/product/micropmu/highlights/

[37] P. Romano and M. Paolone, "Enhanced Interpolated-DFT for Synchrophasor Estimation in FPGAs: Theory, Implementation, and Validation of a PMU Prototype," in IEEE Transactions on Instrumentation and Measurement, vol. 63, no. 12, pp. 2824-2836, Dec. 2014.

[38] Grid Protection Alliance, "Open Source Phasor Data Concentrator", Git repository, 2020, [Online]. Available: https://github.com/GridProtectionAlliance/openPDC

[39] IEEE/IEC International Standard - Measuring relays and protection equipment - Part 118-1: Synchrophasor for power systems - Measurements," in IEC/IEEE 60255-118-1:2018 , vol., no., pp.1-78, 19 Dec. 2018, doi: 10.1109/IEEESTD.2018.8577045.IEEE/IEC International Standard - Measuring relays and protection equipment - Part 118-1: Synchrophasor for power systems - Measurements," in IEC/IEEE 60255-118-1:2018 , vol., no., pp.1-78, 19 Dec. 2018, doi: 10.1109/IEEESTD.2018.8577045.

[40] A. Karimi, C. Kammer, "A data-driven approach to robust control of multivariable systems by convex optimization," Automatica, vol. 85, pp. 227-233, 2017.

[41] B. Miao, R. Zane and D. Maksimovic, "System identification of power converters with digital control through cross-correlation methods," in IEEE Transactions on Power Electronics, vol. 20, no. 5, pp. 1093-1099, Sept. 2005.

[42] K.Zhou and J.C. Doyle, *Essentials of Robust Control*. New Jersey: Prentice Hall, 1998.

[43] J. Löfberg,"YALMIP : A Toolbox for Modeling and Optimization in MATLAB", in *Proc. CACSD Conf.*, Sep. 2004, pp.284-289. [Online]. Available: https://yalmip.github.io/download/

[44] MOSEK ApS. (2015). *The MOSEK Optimization Toolbox for MATLAB Manual. Version 8.1*. [Online]. Available: https://docs.mosek.com/8.1/toolbox/index.html